Available online at www.sciencedirect.com

ScienceDirect

Geochimica et Cosmochimica Acta 120 (2013) 628–647

Geochimica et Cosmochimica Acta

www.elsevier.com/locate/gca

Ba isotopic compositions in stardust SiC grains from the Murchison meteorite: Insights into the stellar origins of large SiC grains

Janaína N. Ávila [a,b,c,*], Trevor R. Ireland [a,b], Frank Gyngard [d], Ernst Zinner [d], Guilherme Mallmann [a,e], Maria Lugaro [f], Peter Holden [a], Sachiko Amari [d]

[a] Research School of Earth Sciences, The Australian National University, Canberra, ACT 0200, Australia
[b] Planetary Science Institute, The Australian National University, Canberra, ACT 0200, Australia
[c] Astronomy Department/IAG, University of São Paulo, São Paulo, SP 05508-090, Brazil
[d] Laboratory for Space Sciences and the Department of Physics, Washington University, One Brookings Drive, St. Louis, MO 63130, USA
[e] Institute of Geosciences, University of São Paulo, São Paulo, SP 05508-080, Brazil
[f] Monash Centre for Astrophysics, Monash University, Clayton, VIC 3800, Australia

Received 14 November 2011; accepted in revised form 28 March 2013; available online 9 April 2013

Abstract

We report barium isotopic measurements in 12 large (7–58 μm) stardust silicon carbide grains recovered from the Murchison carbonaceous chondrite. The C-, N-, and Si-isotopic compositions indicate that all 12 grains belong to the mainstream population and, as such, are interpreted to have condensed in the outflows of low-mass carbon-rich asymptotic giant branch (AGB) stars with close-to-solar metallicity. Barium isotopic analyses were carried out on the Sensitive High Resolution Ion Microprobe – Reverse Geometry (SHRIMP-RG) with combined high mass resolution and energy filtering to eliminate isobaric interferences from molecular ions. Contrary to previous measurements in small (<5 μm) mainstream grains, the analyzed large SiC grains do not show the classical *s*-process enrichment, having near solar Ba isotopic compositions. While contamination with solar material is a common explanation for the lack of large isotopic anomalies in stardust SiC grains, particularly for these large grains which have low trace element abundances, our results are consistent with previous observations that Ba isotopic ratios are dependent on grain size. We have compared the SiC data with theoretical predictions of the evolution of Ba isotopic ratios in the envelopes of low-mass AGB stars with a range of stellar masses and metallicities. The Ba isotopic measurements obtained for large SiC grains from the LS + LU fractions are consistent with grain condensation in the envelope of very low-mass AGB stars (1.25 $M_{\odot}$) with close-to-solar metallicity, which suggests that conditions for growth of large SiC might be more favorable in very low-mass AGB stars during the early C-rich stages of AGB evolution or in stable structures around AGB stars whose evolution was cut short due to binary interaction, before the AGB envelope had already been largely enriched with the products of *s*-process nucleosynthesis.

1. INTRODUCTION

The majority of stardust silicon carbide (SiC) grains (i.e., the so-called mainstream population; ~93% of all SiC) are believed to have condensed in the outflows of low-mass (~1.5–3 $M_{\odot}$), carbon-rich asymptotic giant branch (AGB) stars with close-to-solar metallicity (Hoppe et al., 1994; Zinner et al., 2006). Elemental abundances (e.g., Amari et al., 1995) and isotopic compositions of several heavy trace elements (e.g., Zr, Nicolussi et al., 1997; Mo, Nicolussi et al., 1998a; Sr, Nicolussi et al., 1998b; Ba, Savina et al., 2003; Ru, Savina et al., 2004) measured

* Corresponding author.
E-mail address: janaina.avila@anu.edu.au (J.N. Ávila).

0016-7037/$ - see front matter © 2013 Elsevier Ltd. All rights reserved.
http://dx.doi.org/10.1016/j.gca.2013.03.039

in mainstream SiC grains are, for the most part, consistent with theoretical models of *slow* neutron capture nucleosynthesis (the *s*-process) occurring in the He-intershell of low-mass AGB stars with approximately solar metallicity (e.g., Lugaro et al., 2003).

To date, almost all studies of stardust SiC grains recovered from primitive meteorites have focused on grains of size <5 μm. Exceptions are the studies of Ireland et al. (1991), Virag et al. (1992), Gyngard et al. (2009a,b), Heck et al. (2009) and Ávila et al. (2012, 2013), for which large SiC grains from the Murchison L series, namely the LS + LU fractions (Amari et al., 1994), were analyzed for trace elements as well as He, Li, B, C, N, Ne, Si, Al–Mg, Ti, Eu, and W isotopes. Silicon carbide grains larger than 5 μm represent less than 0.001% of the SiC population in the Murchison meteorite (Amari et al., 1994), and present some unique features. For instance, isotopic compositions show clustering for C and Si (Virag et al., 1992), and even for Ti (Ireland et al., 1991). Concentrations of N, Al, Ti, and other trace elements in most LS + LU grains (Virag et al., 1992) are much lower than those in smaller SiC grains (Hoppe et al., 1994; Amari et al., 1995). Measurements of W isotopic compositions in large SiC grains show small isotopic deviations from solar composition (Ávila et al., 2012). In fact, some grains have normal (=solar) isotopic ratios within errors. Another distinguishing characteristic of LS + LU grains (particularly the larger ones) is their morphology. While most of the smaller SiC grains show euhedral crystal features (e.g., Hoppe et al., 1994; Bernatowicz et al., 2003), a significant fraction of the largest LS + LU grains show blocky appearances, frequently with smooth surfaces. Recently, Gyngard et al. (2009a,b) and Heck et al. (2009) determined that large SiC grains from the LS + LU fractions have interstellar exposure ages ranging from ~3 Ma to ~1 Ga, which implies that the parent stars of the these large grains must have ended their lives within this time range before the formation of the Solar System.

The conditions enabling the formation of such large (in some cases up to 60 μm) SiC grains in stellar outflows are not well understood. Nuth et al. (2006) concluded that growth of large crystalline SiC grains must have occurred deep within the stellar atmosphere, just above the photosphere, of low-mass AGB stars (<3 $M_{\odot}$) where near-equilibrium conditions might have persisted for more than 10^5 years. These conditions, however, cannot be achieved in stellar outflows, where the dynamics of mass loss, temperatures, and densities are rapidly changing. On the other hand, temperatures normally found near photospheres (>2000 K) of low-mass AGB stars are too high to enable condensation of SiC grains (~1700–1400 K). Nuth et al. (2006) also demonstrated that a nearly perfect balance between radiation pressure and stellar gravity, needed to promote long-term stable growth of large grains, is only achieved in low-mass AGB stars. Observational evidence also suggests that grains formed in stellar outflows of AGB stars become progressively smaller as the star evolves (Speck et al., 2005). Other possible sites for the formation of very large dust grains are stable structures such as circumstellar/circumbinary disks and tori where dust is stored around the central star(s) and allowed to grow. These dusty structures and associated large grains are observed around post-AGB binaries (although these are typically O-rich; Gielen et al., 2011) and planetary nebulae (Cerrigone et al., 2009).

In the present work, we report the results of Ba isotopic analyses performed on 12 large (7–58 μm) single stardust SiC grains (LS + LU fractions, Amari et al., 1994) and on a SiC-enriched bulk sample (KJB fraction, Amari et al., 1994) with the ANU Sensitive High Resolution Ion Microprobe – Reverse Geometry (SHRIMP-RG). Barium has seven stable isotopes: the *p*-only pair ^{130}Ba and ^{132}Ba; the *s*-only pair ^{134}Ba and ^{136}Ba; the neutron magic ^{138}Ba, which is mostly of *s*-process origin; and the odd isotopes ^{135}Ba and ^{137}Ba, which are of mixed *r*- and *s*-process origin (Fig. 1). Previous Ba isotopic studies on small SiC grains (<5 μm) have indicated a correlation between the magnitude of isotopic anomaly and grain size (Zinner et al., 1991; Prombo et al., 1993; Savina et al., 2003), with smaller grains having larger deviations from the solar ratios. The present results complement the data obtained by Zinner et al. (1991), Prombo et al. (1993), Savina et al. (2003), Barzyk et al. (2007) and Marhas et al. (2007) in that they include Ba measurements on large (>6 μm) SiC grains.

In addition to the Ba isotopic measurements, we also report on the experimental attempts to produce a synthetic SiC ceramic enriched in trace elements to be used for SHRIMP analyses of heavy elements in stardust SiC grains. This synthetic SiC ceramic, along with other reference materials, was used to delineate possible isobaric mass interferences in the atomic mass region of Ba.

2. SAMPLES, STANDARDS, AND EXPERIMENTAL METHODS

2.1. Stardust silicon carbide grains

Three fractions of SiC grains extracted from the Murchison CM2 carbonaceous chondrite were analyzed in this study, namely KJB (grain size between 0.32 and 0.70 μm), LS (grain size between 2 and 10 μm), and LU (grain size >10 μm). The isolation of the SiC grains from the meteorite matrix was performed by a series of acid digestion and density separation procedures at the University of Chicago (Amari et al., 1994). After separation, grains from the LS and LU fractions were taken up in isopropanol suspensions, deposited on standard microscope slides, and dried. The slides were then visually scanned under an optical microscope. The largest grains were transferred onto a clean Au foil with the help of a micromanipulator, and pressed into the foil with a quartz disk. Imaging and further identification of SiC grains were performed with a scanning electron microscope (SEM) equipped with an energy dispersive X-ray spectrometer. In addition to single-grain analyses, we also carried out measurements on a Murchison SiC-enriched bulk sample (aggregate of many grains from the KJB fraction, Amari et al., 1994). The SiC aggregate was transferred onto a clean Au foil according to the procedure described by Amari et al. (2000). Grains from the KJB fraction have a mass-weighted mean grain size of 0.49 μm. This fraction has been extensively studied, and

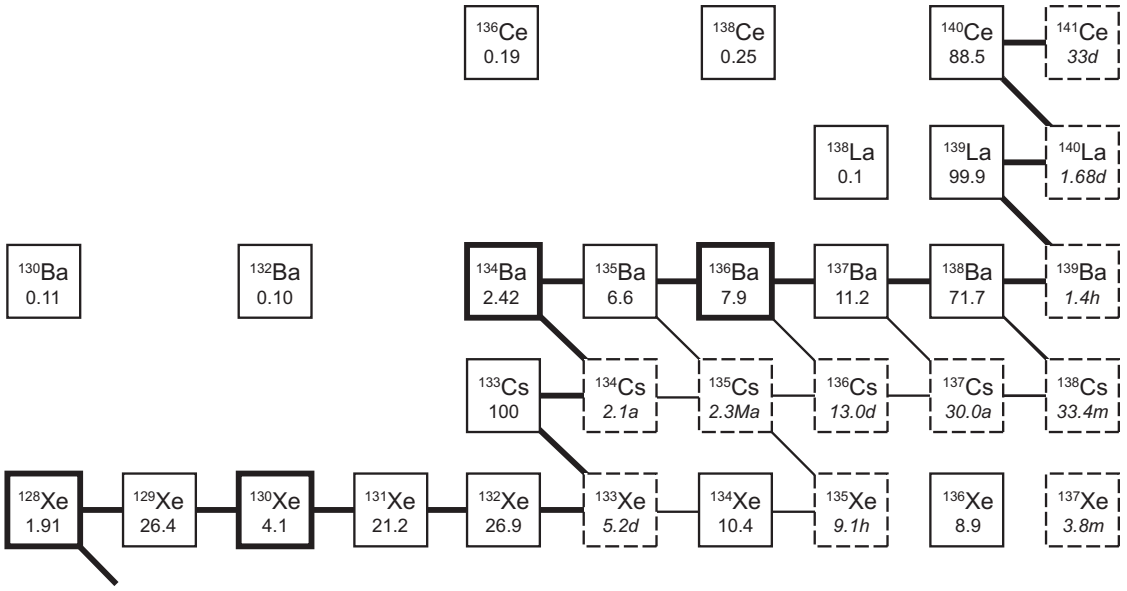

Fig. 1. Part of the chart of nuclides showing the *s*-process nucleosynthesis path in the region of Xe–Cs–Ba–La–Ce. Percent abundances (non-italic) are shown for each stable isotope (solid boxes) and laboratory half-lives (italic) for each unstable isotope (dashed line boxes). The main *s*-process path is shown as a bold line and branches and secondary paths are shown as finer lines; *s*-only isotopes are indicated by bold boxes.

consists of almost pure SiC (~97%; Amari et al., 1994) with relatively high trace-element concentrations (Amari et al., 1995).

2.2. Silicon carbide ceramic enriched in trace elements

The lack of suitable standards for trace element and isotopic measurements in presolar stardust SiC grains makes it extremely difficult to obtain accurate analyses by ion microprobe. Typically, ion microprobe studies of presolar stardust SiC grains make use of silicate glass reference materials doped with the element(s) of interest. However, these materials (e.g., NIST SRM silicate glasses) fail to match the major element composition and structure found in stardust SiC grains. The exceptions are isotopic measurements of C and Si, for which synthetic SiC grains have been used successfully. For measurements of heavy elements, however, there is no natural or synthetic SiC reference material available. Naturally occurring and synthetic samples of SiC contain extremely low abundances of trace elements (except for stardust SiC grains) and are therefore not suitable as standards.

Ion implanted materials have been used as standards for calibration of secondary ion mass spectrometers (e.g., Simons et al., 2007). However, these materials are only useful if the range (i.e., depth) and spatial distribution of the implanted ions are larger than the volume being analyzed. Due to its higher density, the range of dopant ions in SiC is ~2 times smaller than in Si. High ion energies, often in the MeV range, are therefore required to implant ions to just ~1 μm depth in SiC. An additional complication of this technique is that, for high ion energies, the projected range decreases with increasing mass of the ions (e.g., Rao, 2003). The solubility of trace elements in SiC is known empirically to be extremely low, so that crystallization in the laboratory of large SiC crystals containing sufficient concentration of trace elements in solid solution is extremely difficult. However, SiC-based ceramics sintered with desirable amounts of trace elements are relatively easy to produce. These materials can be very helpful in ion microprobe studies of presolar SiC grains, particularly if the sintered material is homogeneous at an appropriate scale. For the purpose of the Ba measurements reported in this study, this scale is about 30 μm (Fig. 2), based on the fact that the SHRIMP O_2^- primary beam was focused to sputter an area of ~30 μm in diameter at the target (see details in Section 2.4).

In order to determine elemental yields and assess the contribution of molecular interferences in ion microprobe analyses of stardust SiC grains, we prepared a SiC ceramic doped with several trace elements at nominal concentrations between 1 and 3000 μg/g. Fine-grained (⩽5 μm) reagent-grade SiC powder was mechanically mixed with several trace elements (Y, Ba, REE, W, Pb, Th, and U), introduced as either oxide (Y_2O_3, REE_2O_3, and U_3O_8), nitrate ($Ba(NO_3)_2$ and $Th(NO_3)_4{\cdot}4H_2O$), carbide (WC), or sulphide (PbS). The mixed material was ground manually in an agate mortar under acetone for about 30 min, pressed into a pellet, and then fired in air at 1050 °C for ~10 h to drive off the volatiles. The pellet was then reground under acetone for another 30 min, dried, loaded into a graphite-lined 2.7 mm-diameter Pt capsule, and weld-sealed. The material was contained in a graphite capsule to avoid oxidation of the components. The experimental charge was run in a piston-cylinder apparatus using a ½-inch NaCl, Pyrex, graphite, MgO assembly at 3 GPa and 1400 °C for approximately 10 min. The objective of this procedure was solely to remove pore space and hence to produce a material (a ceramic) as homogeneous as possible at the 30 μm scale (SHRIMP spot sizes chosen in the present study). Quenching was achieved by shutting the power

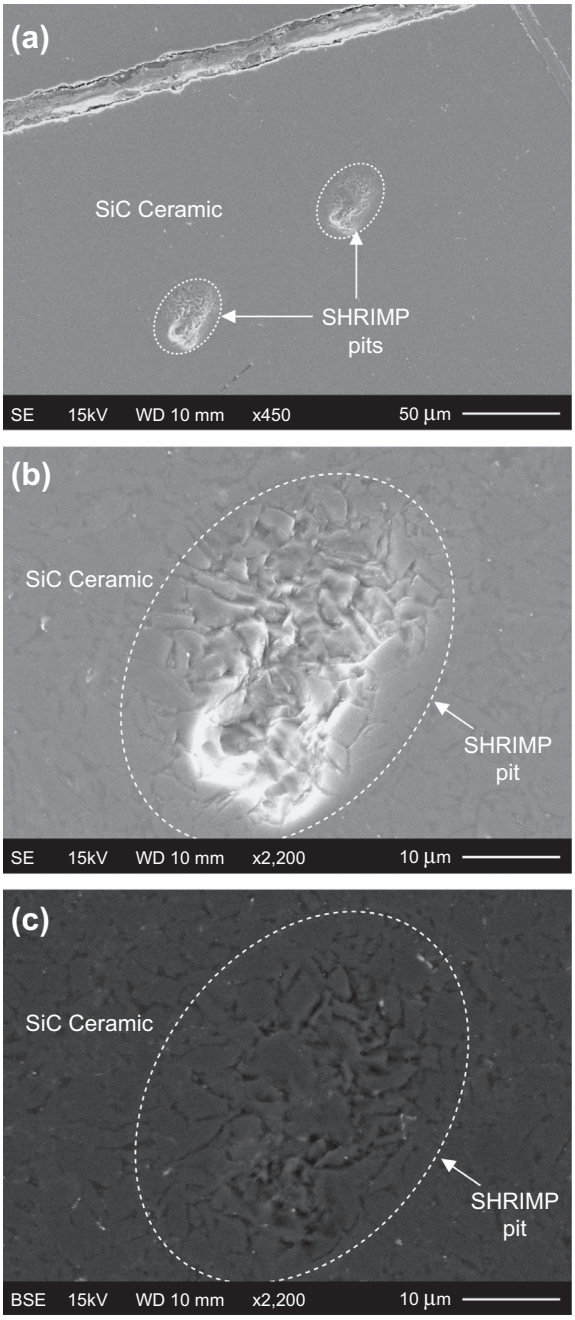

Fig. 2. (a) Secondary electron image (SE) of the silicon carbide ceramic enriched in trace elements after sputtering of two areas in the ion probe. A high-magnified area containing one of the sputter pits is shown in (b); (c) backscattered electron image (BSE) of the area shown in (b). The ceramic has an average grain-size of about 5 µm, with grain boundaries being accentuated after sputtering. Brighter spots are enriched in oxygen relative to the surrounding silicon carbide, but no elements other than Si, C, and O are observed in the EDX spectrum.

off. The relatively short run time was chosen to avoid unmixing between the components and consequent formation of additional phases.

High magnification secondary electron (SE) and backscattered electron (BSE) images were obtained for the SiC ceramic (Fig. 2). Energy dispersive X-ray (EDX) spectra were also taken in several spots of the SiC ceramic in order to obtain information on homogeneity and bulk composition. Only Si and C, and occasionally O peaks, were identified by EDX.

The absolute abundances of trace elements in the SiC ceramic and in a "pure" synthetic SiC single crystal were determined by Laser Ablation – Inductively Coupled Plasma – Mass Spectrometry (LA-ICP-MS) at the Australian National University. The system consists of an ArF (193 nm wavelength) excimer laser, which is interfaced to a custom-built sample cell (HelEx) and then to a quadrupole Agilent 7500s ICP-MS (Eggins et al., 1998). Ablation was performed in a He–Ar atmosphere with a pulse energy of ~60 mJ and pulse repetition rate of 5 Hz. The laser was focused to a spot size of 35 µm, and the acquisition time per spectrum was set to 60 s (20 s for counting the background followed by 40 s for counting the ablation signal). The ablated material was flushed in a continuous Ar flow into the torch of the ICP-MS. Before and after analysis of ten unknowns, the silicate glass reference material NIST-610 was measured for external calibration and to perform instrumental drift corrections. To correct for differences in ablation efficiency between external standard and samples, ^{29}Si was used as the internal abundance reference based on its stoichiometric proportion in SiC. The abundances in µg/g of trace elements in the SiC ceramic are reported in Table 1.

2.3. Carbon, nitrogen, and silicon isotopic measurements

Carbon-, N-, and Si-isotopic ratios for the KJB fraction have been previously reported by Amari et al. (2000) and are reproduced in Table 2. These measurements were performed with a modified Cameca IMS-3f ion microprobe at Washington University in St. Louis. The LS + LU grains were analyzed for their C-, N-, and Si-isotopic compositions (Table 2) with a Cameca NanoSIMS at Washington University. The NanoSIMS measurements were performed by rastering a ~100 nm Cs^+ primary beam (~1 pA) over a sample area of 2–10 µm^2 while SEs and negative secondary ion species were collected. Electron multipliers were used for the simultaneous detection of $^{12}C^-$, $^{13}C^-$, $^{28}Si^-$, $^{29}Si^-$, and $^{30}Si^-$. The acquisition time for each grain was ~4 min, consisting of 10 cycles with 10 measurements each. Subsequent to the C- and Si-isotopic measurements, nitrogen isotopes were measured as CN^- ions at masses 26 ($^{12}C^{14}N^-$) and 27 ($^{12}C^{15}N^-$) (Zinner et al., 1989). During the acquisition of nitrogen isotopes, $^{12}C^-$, $^{13}C^-$, and $^{30}Si^-$ were measured again, simultaneously with the CN^- species. The acquisition time was ~4 min. The positions of all mass peaks were routinely checked. Since the measurements were acquired in multi-collection mode, the magnetic field remained static during the entire analysis. A synthetic SiC was used for normalization of the C and Si isotopes, while a fine-grained mixture of SiC and Si_3N_4 was used for calibration of the N isotopes.

Table 1
Trace-element composition (μg/g) of synthetic SiC determined by LA-ICP-MS.

	SiC ceramic			"pure" Synthetic SiC		
	Mean	SD	*n*	Mean	SD	*n*
Li(7)	<0.1	n/a	12	<0.02	n/a	3
Be(9)	<0.1	n/a	12	<0.08	n/a	3
B(11)	10.6	1.5	12	1.66	0.07	3
Na(23)	31	10	12	0.74	0.19	3
Mg(25)	29.7	3.4	12	0.90	0.10	3
Al(27)	281	59	30	45.5	5.5	3
P(31)	14.7	2.2	12	3.7	0.2	3
K(39)	26.9	6.0	12	<0.7	n/a	3
Ca(43)	121	20	12	109	6	3
Sc(45)	5.1	0.7	12	1.77	0.02	3
Ti(47)	324	105	12	1.93	0.25	3
V(51)	215	19	12	2.70	0.23	3
Cr(53)	14.7	7.6	12	1.84	0.10	3
Mn(55)	3.3	1.1	12	0.03	0.01	3
Fe(57)	379	180	12	0.72	0.27	3
Co(59)	9.5	5.5	12	<0.01	n/a	3
Ni(60)	85	40	12	<0.10	n/a	3
Cu(63)	4.5	1.1	12	<0.02	n/a	3
Zn(66)	9.1	1.2	12	<0.06	n/a	3
Ga(71)	11.4	2.4	12	<0.01	n/a	3
Ge(72)	7.3	0.4	12	<0.60	n/a	3
As(75)	2.7	3.3	12	<0.20	n/a	3
Rb(85)	0.11	0.02	12	<0.01	n/a	3
Sr(88)	0.46	0.06	12	<0.002	n/a	3
Y(89)	1.15	0.62	12	<0.002	n/a	3
Zr(90)	32	10	12	<0.009	n/a	3
Nb(93)	0.75	0.15	12	<0.003	n/a	3
Mo(95)	2.46	0.38	12	<0.020	n/a	3
Ru(101)	<0.1	n/a	12	<0.005	n/a	3
Ba(138)	3054	195	45	<0.030	n/a	3
La(139)	522	90	45	<0.007	n/a	3
Ce(140)	445	39	45	<0.003	n/a	3
Pr(141)	484	37	45	<0.003	n/a	3
Nd(146)	279	20	45	<0.020	n/a	3
Sm(147)	276	19	45	<0.030	n/a	3
Eu(153)	60.7	3.4	45	<0.006	n/a	3
Gd(157)	13.8	3.8	45	<0.045	n/a	3
Tb(159)	0.055	0.012	45	<0.003	n/a	3
Dy(163)	0.27	0.08	45	<0.015	n/a	3
Ho(165)	16.4	8.0	45	<0.008	n/a	3
Er(166)	0.21	0.06	45	<0.015	n/a	3
Tm(169)	7.28	2.48	45	<0.004	n/a	3
Yb(172)	5.80	0.40	45	<0.020	n/a	3
Lu(175)	4.43	0.96	45	<0.007	n/a	3
Hf(178)	1.21	0.28	28	<0.025	n/a	3
Ta(181)	0.51	0.16	28	<0.005	n/a	3
Os(189)	<0.1	n/a	28	<0.005	n/a	3
W(182)	1828	191	45	<0.020	n/a	3
Pb(208)	845	147	45	<0.015	n/a	3
Th(232)	1742	88	45	<0.015	n/a	3
U(238)	359	24	45	<0.005	n/a	3

SD = standard deviation (1σ); *n* = number of data points analyzed; n/a = not applicable. The masses of the isotopes analyzed are given next to the elements.

2.4. Barium isotopic measurements

Barium isotopic analyses were carried out with the SHRIMP-RG at the Australian National University. Mass scans on several samples (Fig. 3) were taken at a mass resolving power of $m/\Delta m = 5000$ (at 10% peak) to establish the existence and contribution of mass interferences at $^{134}Ba^+$, $^{135}Ba^+$, $^{136}Ba^+$, $^{137}Ba^+$, and $^{138}Ba^+$. Barium-130 and ^{132}Ba were not investigated due to their low isotopic abundances. We analyzed a nominally "pure" synthetic SiC with undetectable amounts of trace elements (Table 1), a SiC ceramic enriched in trace elements (Section 2.2), and a large stardust SiC grain (grain WU-06, Table 2). In addition, mass scans were taken from two standard reference silicate materials, the synthetic silicate glass NIST-610 from the National Institute of Standards and Technology (NIST), and the natural Columbia River basaltic glass BCR-2G from the United States Geological Survey (USGS).

The mass scans revealed a number of significant molecular interferences, particularly affecting ^{134}Ba and ^{136}Ba. However, these interferences were not evident in silicate matrices, as shown by mass scans obtained from the NIST-610 and BCR-2G silicate glasses (Fig. 3). This suggests that the interferences come from molecular ions involving major elements from the SiC matrix (e.g., $^{28}Si_4{}^{12}C_2$ has a nominal mass of 136 and its resolution from $^{136}Ba^+$ requires a mass resolving power of 43,000). The mass offsets between the atomic species ($^{134}Ba^+$, $^{135}Ba^+$, $^{136}Ba^+$, $^{137}Ba^+$, and $^{138}Ba^+$) and their corresponding molecular interferences are too small to be resolved by mass separation without drastically compromising the secondary ion detection efficiency. Therefore, to suppress molecular ion contributions to the atomic species, we used an energy filtering technique (Steele et al., 1977; Zinner and Crozaz, 1986; Fahey, 1998). While an energy window is routinely used after the electrostatic analyzer (ESA) in SHRIMP-I and II to select a distinct energy range for the total secondary ion beam, the methodology for SHRIMP-RG relies on selection of an appropriate energy range on the basis of the momentum spectrum obtained after the magnet (and preceding the ESA). In this case, there is a unique correspondence between the energy spectrum and the momentum spectrum only for the given mass of interest. For an energy offset of approximately 24 eV, selected based on the momentum spectrum at mass region 134 a.m.u. of ions sputtered from the NIST-610 silicate glass and a "pure" synthetic SiC (Fig. 4), we observed that molecular interferences were completely excluded from the collected ions (Fig. 3b, d, f, h and j); however, the ion intensity loss is a factor of 5 for the Ba isotopes. We did not acquire mass scans for the stardust SiC grain (WU-06) with energy filtering, as we decided to preserve this grain for further isotopic measurements.

Similar to some previous Ba isotopic studies (e.g., Savina et al., 2003; Marhas et al., 2007), the stardust SiC grains analyzed here had been previously bombarded with Cs, as a Cs^+ primary ion beam was used for the C-, N-, and Si-isotopic measurements. The result of these measurements is a considerable amount of implanted ^{133}Cs on the surface of the grains, which could potentially interfere (as CsH_x) with Ba isotopic measurements. The contribution of CsH_x interferences on the Ba isotopes should, however, decrease as the mass increases. This is because the mass difference

Table 2
C-, N-, Si-, and Ba-isotopic compositions of stardust SiC grains from the KJB and LS + LU fractions. Errors are 1σ.

Grain/ spot	Morph.[b]	Size (μm)	$^{12}C/^{13}C$	$^{14}N/^{15}N$	$\delta^{29}Si/^{28}Si$[c] (‰)	$\delta^{30}Si/^{28}Si$[c] (‰)	Energy offset (eV)	$\delta^{134}Ba/^{136}Ba$[d] (‰)	$\delta^{135}Ba/^{136}Ba$[d] (‰)	$\delta^{137}Ba/^{136}Ba$[d] (‰)	$\delta^{138}Ba/^{136}Ba$[d] (‰)	Ba^{SiC} (μg/g)	Ba^{NIST} (μg/g)
KJB fraction (Murchison SiC-enriched sample)													
KJB[a]		0.49	37 ± 0.4	521 ± 60	24.6 ± 1.3	37.8 ± 3.4	0	81 ± 97	−477 ± 42	−310 ± 43	−215 ± 52		
							24	140 ± 13	−423 ± 2	−284 ± 5	−281 ± 23	380	248
LS + LU fractions (Murchison single grains)													
WU-1	E	8 × 9	57.5 ± 0.4	434 ± 24	98.6 ± 5.4	73.5 ± 9.7	0	−23 ± 34	−253 ± 26	−251 ± 24	−285 ± 38		
							24	−30 ± 71	7 ± 54	−31 ± 47	−35 ± 74	10.3	6.5
WU-3	A	10 × 12	48.3 ± 0.3	462 ± 36	38.4 ± 4.7	51.4 ± 9.1	0	−757 ± 28	−715 ± 26	−597 ± 26	−703 ± 16		
							24	116 ± 165	−177 ± 100	−79 ± 95	−54 ± 99	1.7	1.0
WU-4	A	26 × 34	49.3 ± 0.4	305 ± 14	32.4 ± 4.8	29.9 ± 9.1	24	−32 ± 60	−7 ± 71	−38 ± 62	−76 ± 114	10.4	6.6
WU-5	E	6 × 8	84.2 ± 0.6	n.a.	9.0 ± 4.6	31.9 ± 9.0	0	−86 ± 110	−184 ± 75	−15 ± 71	−232 ± 49		
							24	224 ± 143	57 ± 97	19 ± 84	−21 ± 92	6.8	4.3
WU-6	E	10 × 11	61.5 ± 0.5	568 ± 22	34.8 ± 5.0	28.9 ± 9.2	0	−144 ± 30	−378 ± 22	−311 ± 21	−450 ± 34		
							24	27 ± 105	−50 ± 72	−109 ± 60	−152 ± 73	5.9	3.7
WU-8	A	30 × 58	48.4 ± 0.3	306 ± 17	43.6 ± 4.7	53.9 ± 9.1	0	−483 ± 33	−631 ± 30	−661 ± 37	−774 ± 21		
							24	−20 ± 83	39 ± 62	−95 ± 50	−25 ± 77	3.0	1.9
WU-9	E	8 × 13	78.5 ± 0.6	427 ± 9	33.0 ± 4.9	32.3 ± 9.2	24	−29 ± 69	−32 ± 50	−26 ± 45	−48 ± 72	10.3	6.5
WU-10	A	7 × 14	90.8 ± 0.7	287 ± 10	10.1 ± 4.6	11.1 ± 8.8	0	−323 ± 36	−364 ± 27	−303 ± 24	−288 ± 26		
							24	56 ± 94	−83 ± 63	−108 ± 54	−69 ± 76	6.1	3.8
WU-13	A	7 × 12	48.7 ± 0.3	341 ± 23	32.9 ± 4.7	46.6 ± 9.1	0	−634 ± 25	−674 ± 20	−560 ± 20	−618 ± 36		
							24	−78 ± 102	82 ± 98	−12 ± 61	20 ± 93	2.8	1.8
WU-18	A	13 × 18	49.7 ± 0.3	310 ± 7	38.7 ± 4.7	43.7 ± 9.1	0	−531 ± 12	−532 ± 40	−514 ± 10	−553 ± 47		
							24	−138 ± 69	−63 ± 54	63 ± 55	130 ± 89	3.3	2.0
WU-19	E	9 × 13	57.6 ± 0.4	296 ± 5	63.6 ± 5.0	44.9 ± 9.2	0	92 ± 69	−180 ± 52	−185 ± 44	−278 ± 81		
							24	205 ± 79	123 ± 58	108 ± 53	−215 ± 61	5.1	3.2
WU-52	E	6 × 7	76.0 ± 0.7	661 ± 38	35.1 ± 5.7	38.4 ± 9.8	24	−222 ± 106	−93 ± 56	−137 ± 87	−144 ± 97	5.0	3.1

Ba^{SiC} and Ba^{NIST} correspond to the Ba abundances determined for stardust SiC grains using the SiC ceramic and NIST-610 silicate glass as normalization standard, respectively.

[a] C-, N-, and Si-isotopic data of grains from KJB fraction reproduced from Amari et al. (2000).

[b] Morphologies according to Virag et al. (1992): A = anhedral, blocky, smooth surfaces and E = round to irregular, euhedral features, bounded by one or more crystal faces.

[c] $\delta^{i}Si/^{28}Si\ (‰) = [(^{i}Si/^{28}Si)_{measured}/(^{i}Si/^{28}Si)_{solar} - 1] \times 10^{3}$.

[d] $\delta^{i}Ba/^{136}Ba\ (‰) = [(^{i}Ba/^{136}Ba)_{measured}/(^{i}Ba/^{136}Ba)_{solar} - 1] \times 10^{3}$.

(Δm) observed between the Ba isotopes and CsH_x molecules increases from 0.0087 (Δm between $^{134}Ba^+$ and $^{133}CsH^+$) to 0.0393 a.m.u. (Δm between $^{138}Ba^+$ and $^{133}CsH_5^+$). Furthermore, hydride signals are expected to decrease with increasing number of hydrogen atoms in the molecule. In addition, in the stardust SiC grains, the CsH_x interferences should decrease as a function of analysis time as more and more of the layer implanted with Cs^+ is sputtered away by the primary O_2^- beam. CsH_x interferences are well resolved from ^{136}Ba, ^{137}Ba, and ^{138}Ba at a mass resolving power of $m/\Delta m = 5000$. However, a much higher mass resolving power ($m/\Delta m > 8500$) is necessary to resolve ^{134}Ba and ^{135}Ba from CsH_x.

The interference observed at mass 134 in the stardust SiC grain (Fig. 3a) is at the same position as that expected for $^{133}CsH^+$. However, an interference at the same mass position is also observed in the "pure" synthetic SiC, which has undetectable amounts of Cs (Fig. 5). This interference also has identical peak intensity (cps/s/nA) relative to that observed in the stardust grain (Fig. 3a). Given that the concentration of Cs is extremely variable among these samples (i.e., "pure" synthetic SiC, SiC ceramic, and stardust SiC grain) it seems unlikely that an interference arising from CsH^+ would result in peaks with exactly the same intensity in all SiC matrices. Furthermore, a tail at the high mass side of $^{134}Ba^+$ would also be expected for the NIST-610 silicate glass ($^{133}Cs = 361$ μg/g; Pearce et al., 1997) if CsH^+ were indeed an important interference. From Fig. 3a, we observe that this is not the case. The relatively small energy offset (~24 eV) sufficient to suppress the unwanted interferences in the mass region of interest also suggests that these interferences result from polyatomic species, probably with four or more constituent atoms (e.g., $^{28}Si_4{}^{12}C_2$, $^{28}Si_3{}^{29}Si^{12}C_2$, $^{28}Si_2{}^{29}Si_2{}^{12}C_2$). The energy offset employed here is, however, not sufficient to remove hydrides.

In order to quantify the contribution of interferences to the Ba isotopic ratios measured in stardust SiC grains by ion microprobe, we chose to analyze stardust SiC grains with two distinct setups, one with (energy offset of ~24 eV) and the other without (energy offset of 0 eV) energy filtering. Barium isotopic measurements were performed with an O_2^- primary beam of ~4 nA focused to sputter an area of ~30 μm in diameter. Before data acquisition, each spot/grain was initially sputtered by the primary beam rastered over an area slightly larger (~60 μm in diameter) than the analytical spot for ~60 s to minimize surface contamination. Secondary ions were extracted at 10 keV and measured by single collector analysis on the ETP™ multiplier in magnetic peak-jumping mode. SHRIMP-RG was operated at a mass resolving power of $m/\Delta m = 5000$ (at 10% peak height). The acquisition time for each grain was ~8 min, which consisted of five cycles through the following peaks: $^{134}Ba^+$, $^{135}Ba^+$, $^{136}Ba^+$, $^{137}Ba^+$, $^{138}Ba^+$, $^{139}La^+$, and $^{140}Ce^+$. We systematically bracketed three unknowns by a suite of standard reference materials: NIST-610 and BCR-2G silicate glasses, SiC ceramic doped with trace elements, and "pure" synthetic SiC.

It is important to note that there are other potential isobaric interferences at $^{136}Ba^+$ from $^{136}Ce^+$ and at $^{138}Ba^+$ from $^{138}La^+$ and $^{138}Ce^+$. However, in the Solar System, these are rare isotopes of La ($^{138}La = 0.090\%$ of solar La) and Ce ($^{136}Ce = 0.185\%$ and $^{138}Ce = 0.251\%$ of solar Ce) and, therefore, much less abundant than ^{136}Ba and ^{138}Ba. Also, these isotopes, which lie outside the *s*-process path (Fig. 1), are not produced by *s*-process nucleosynthesis in low mass AGB stars, thus their abundance in SiC grains from AGB stars should be very low (assuming that the SiC grains have a strong *s*-process signature). By measuring $^{139}La^+$ and $^{140}Ce^+$ together with the Ba isotopes, we found that interferences from La and Ce isobars were negligible and no correction was applied.

From Fig. 6, it is clear that during a typical SHRIMP analysis of single stardust SiC grains, because the sputter rate of Au is much higher than that of SiC, most of the material that is sputtered by the primary beam comes from the substrate onto which the grains are deposited rather than from the grains themselves. We have periodically investigated the purity of the Au substrate on which the SiC were deposited, but found no detectable contamination. Examination of the grains' surfaces by high magnification field emission scanning electron microscope (FESEM) revealed that no other mineral grains (contaminants) were in contact with the stardust grains. Hence, all detected Ba is likely intrinsic to the stardust SiC grains.

The NIST-610 silicate glass and the SiC ceramic enriched with trace elements were used to determine instrumental mass fractionation (IMF) correction for Ba isotopic ratios measured in the unknowns. The IMF values calculated from analyses of both standards are in agreement with each another within two-sigma (2σ) error. The Ba isotopic results obtained with SHRIMP-RG in single-collection mode were corrected by using Dodson's (1978) double-interpolation algorithm; a time interpolation algorithm that makes allowance for non-linear variations of signal intensity with time during cyclical scanning of a series of mass peaks. Uncertainties due to the dispersion (i.e., standard deviation) of measurements on the standards during the analytical session were calculated from repeated analyses of NIST-610 and SiC ceramic and propagated into the uncertainties of each unknown.

3. RESULTS

3.1. Carbon, nitrogen, and silicon isotopic compositions

As can be seen in Fig. 7, the C-, N-, and Si-isotopic compositions of the SiC grains investigated here are clearly similar to those previously measured in grains from the LS + LU fractions (Virag et al., 1992; Gyngard et al., 2009b; Heck et al., 2009). The LS + LU SiC grains studied here show Si-, C-, and N-isotopic compositions in the range displayed by the so-called "mainstream grains" (Fig. 7 and Table 2), and therefore are believed to have condensed in the outflows of low mass (~1.5–3 $M_\odot$) carbon-rich AGB stars with close-to-solar metallicity (Hoppe et al., 1994; Zinner et al., 2006). The KJB fraction also shows C-, N-, and Si-isotopic signatures consistent with an AGB origin for most of the grains (Amari et al., 2000).

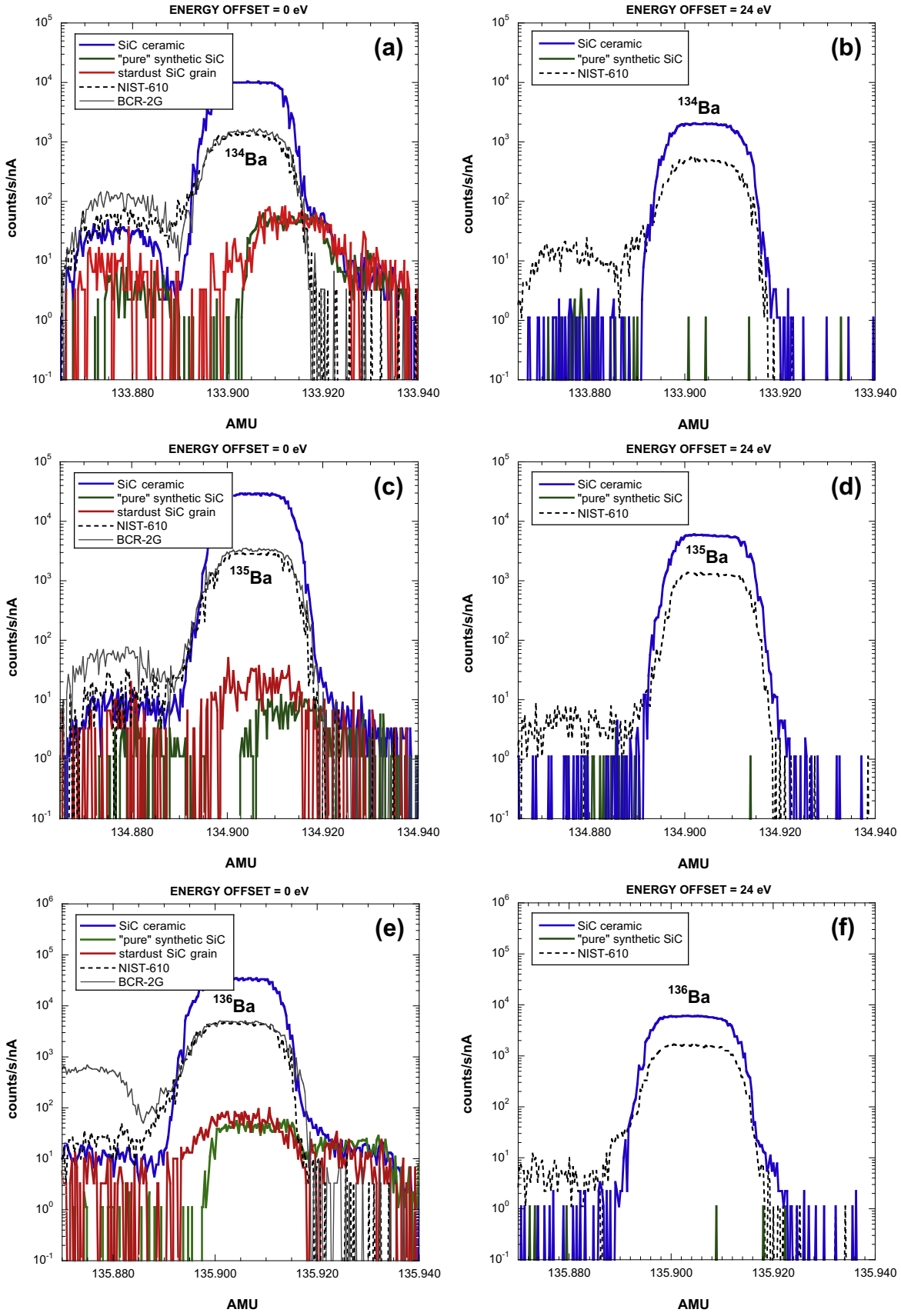

Fig. 3. SHRIMP-RG mass scans of $^{134}Ba^{+}$ (a and b), $^{135}Ba^{+}$ (c and d), $^{136}Ba^{+}$ (e and f), $^{137}Ba^{+}$ (g and h), and $^{138}Ba^{+}$ (i and j), obtained for SiC and silicate matrices with energy offsets of 0 and 24 eV.

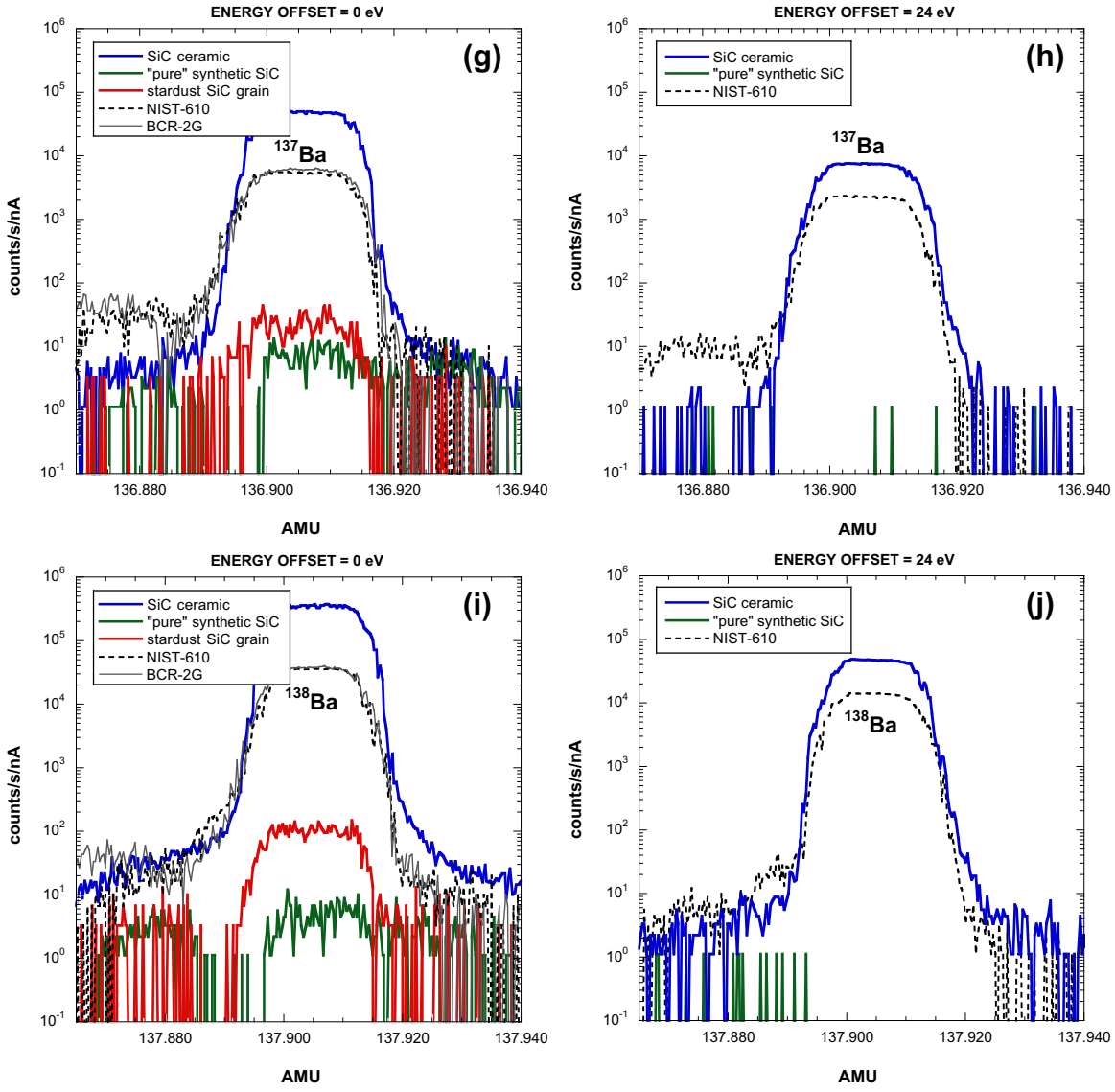

Fig. 3. (*continued*)

3.2. Barium elemental abundances

Barium concentrations obtained with SHRIMP-RG in single stardust SiC grains range from ~2 to 10 μg/g (Table 2). The SiC-enriched sample (KJB fraction) has a Ba abundance of 380 μg/g. The stardust data were normalized to the SiC ceramic (with Ba concentrations independently determined by LA-ICP-MS; Table 1) and NIST-610 silicate glass. The Ba concentration determined for the KJB fraction in this study based on the SiC ceramic as normalization standard is higher than that reported by Zinner et al. (1991; 243 ± 28 μg/g). However, when our KJB data are normalized to the NIST-610 silicate glass, the Ba concentration is 248 μg/g, in excellent agreement with that determined by Zinner et al. (1991). It should be noted that the calculation of Ba concentration in stardust SiC grains is somewhat uncertain because of the lack of a SiC standard that contains Ba in solid solution and is homogeneously distributed at nanometric scale. We do not know whether Ba in our SiC standard is restricted to Ba oxide located between individual SiC crystallites or whether it diffused into the SiC during sintering. This introduces an uncertainty in the determination of the absolute Ba concentration.

Another uncertainty results from the fact that Ba and Si were not measured in the same analysis cycle. Previous measurements of trace-element concentrations by SIMS have compared the ion yields of the elements of interest relative to that of Si in the unknowns with those in standard silicate glasses. Since automatic peak centering is problematic when measuring samples with very low concentrations of trace elements by SHRIMP, the magnetic field stability during the analytical session takes priority. The mass jump from mass 28 ($^{28}Si^{+}$) to 134 ($^{134}Ba^{+}$, first mass measured in our Ba routine) is considerable and is likely to cause problems in magnet hysteresis and therefore peak position, resulting in additional errors in the isotopic yields measured. We

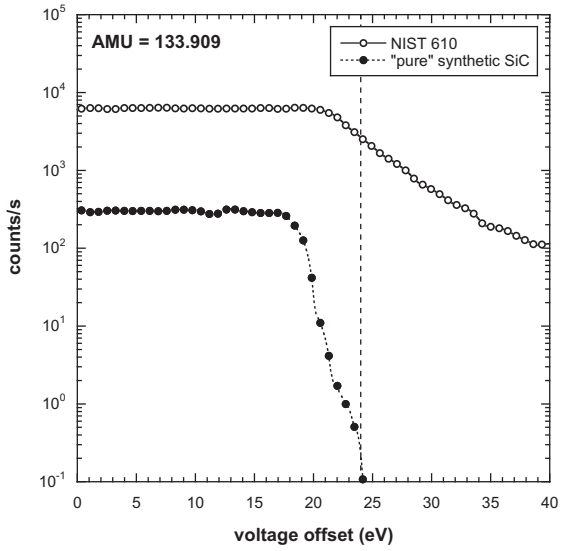

Fig. 4. Momentum spectra at mass region 134 of secondary ions sputtered from the NIST-610 silicate glass and "pure" synthetic SiC obtained with SHRIMP-RG. At an energy offset ~24 eV (dashed line), molecular interferences from the SiC sample are essentially excluded from collection. The spectra were obtained with the energy slit wide open to maximize count rates, which resulted in a flat spectrum at low energies. The energy offset is calculated relative to the maximum ion transmission position (0 eV).

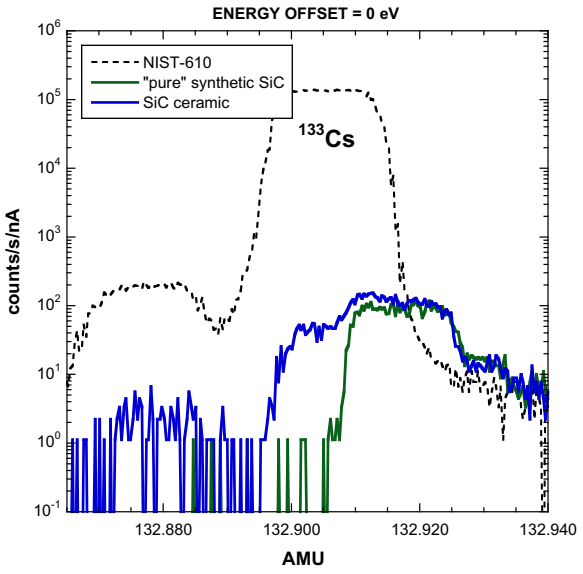

Fig. 5. SHRIMP-RG mass scans of the region around $^{133}Cs^{+}$ obtained from a "pure" synthetic SiC, a SiC ceramic enriched in trace elements, and the NIST-610 silicate glass. Energy offset = 0 eV.

decided that a limited mass range (from 134 to 140) should help in keeping the mass positions almost constant during the analytical session, which was confirmed by regularly checking the mass positions in the standard materials. As a result of our approach, we could not normalise the Ba secondary ion yields for each unknown-standard pair to that of Si. Instead, the elemental concentrations had to be calculated by comparing the counts/s/nA obtained for each single grain with those measured on the synthetic SiC ceramic, assuming normal isotopic ratios for standards and stardust grains, as the stardust SiC grains analysed here display close to solar Ba isotopic ratios (Section 3.4). The obtained values (i.e., concentrations) were further adjusted for the size of each single grain (i.e., the ratio between ion beam area/grain area). This obviously introduces a large uncertainty because it is difficult to predict the 3-dimensional shape of the grains pressed into the Au substrate, and the change in ion yields due to sputtering during the analysis. This uncertainty might be even larger deriving from the fact that we do not know whether Ba in the SiC standard is located between SiC crystallite or is in solid solution within the SiC. In any case, the determination of absolute Ba abundances in the stardust SiC grains is not a major objective of this study. Furthermore, relative abundances between individual grains do not depend on the choice of a calibration standard. We therefore have not pursued the measurement of absolute Ba abundances in more detail.

3.3. Barium isotopic compositions: standards

In Fig. 8a we show Ba isotopic compositions (uncorrected for mass fractionation) determined by multiple measurements of the NIST-610 silicate glass, the SiC ceramic enriched with trace elements, and "pure" synthetic SiC during the course of an analytical session using an energy offset of 0 eV. Barium isotopic ratios are expressed as deviations from the solar isotopic ratio in permil (δ-values) normalized to ^{136}Ba. The ratios measured on the "pure" synthetic SiC are the result of molecular interferences at mass positions similar to those of Ba isotopes. The patterns arise from the fact that interferences are proportionately larger at atomic masses 134 and 136.

The interferences outlined previously on ^{134}Ba and ^{136}Ba do not seem to affect significantly the Ba isotopic ratios measured in the SiC ceramic, probably because of its high (3054 μg/g) Ba concentration. This is obviously not the case for the "pure" synthetic SiC, for which the interferences completely dominate the secondary ion signals. The large fluctuations in the 134/136 ratios observed in the "pure" synthetic SiC (Fig. 8a) may be explained by small shifts (<0.004 a.m.u.) in peak positions during the analytical sessions as the left side shoulder of the interference peak at mass 134 is positioned at the center of the ^{134}Ba peak. In this case, any fluctuation on peak position can easily have a large effect on the secondary ion signal being measured. The non-solar 135/136, 137/136, and 138/136 ratios are consistent with a major interference on mass 136.

The variations in Ba isotopic ratios observed for measurements carried out with and without energy filtering on the SiC ceramic and NIST-610 silicate glass are small and the ratios are, within two-sigma (2σ) errors, all solar. No secondary ions were detected at masses $^{134}Ba^{+}$, $^{135}Ba^{+}$, $^{136}Ba^{+}$, $^{137}Ba^{+}$, and $^{138}Ba^{+}$ in the "pure" synthetic SiC when using an energy offset of 24 eV.

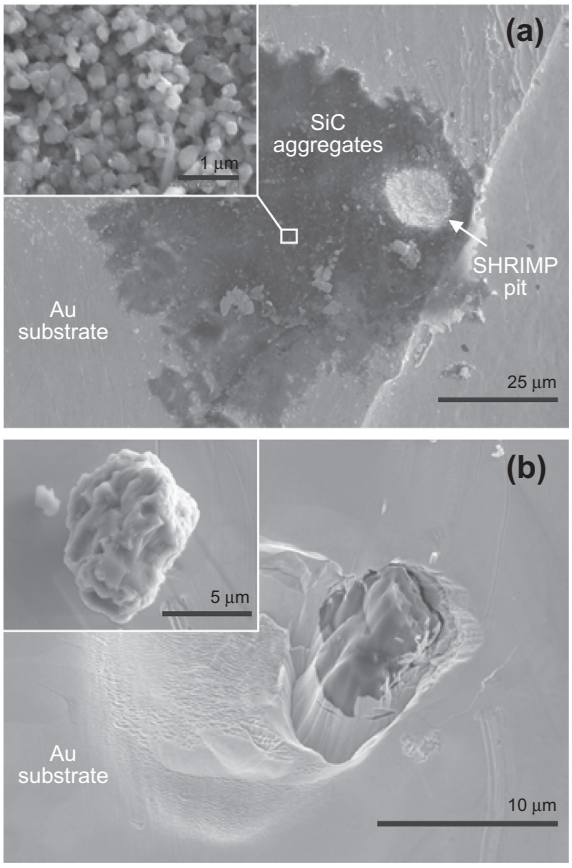

Fig. 6. Secondary electron images showing typical sputtering pits of SiC on gold. (a) Aggregate of presolar SiC grains (dark grey patch) of the KJB fraction deposited on Au substrate. A high-magnification image is shown in the top-left corner. (b) Single stardust SiC grain after 12 min (primary beam current ~4 nA) of O_2^- sputtering; the same grain before SHRIMP analysis is shown in the top-left corner.

3.4. Barium isotopic compositions: stardust SiC grains

Barium isotopic analyses were carried out on 12 large stardust SiC grains (LS + LU fractions) and the SiC-enriched bulk sample (KJB fraction) with energy offsets of 0 and 24 eV, for comparison. The results are given in Table 2. The Ba isotopic patterns of single stardust SiC grains are shown in Fig. 8b and c. The range in Ba isotopic compositions observed in SiC grains analyzed with energy filtering (Fig. 8c) is clearly more restricted and closer to solar than that observed for grains analyzed without energy filtering (Fig. 8b), which show more extreme isotopic compositions. The low $^{134}Ba/^{136}Ba$, $^{135}Ba/^{136}Ba$, $^{137}Ba/^{136}Ba$, and $^{138}Ba/^{136}Ba$ ratios observed in Fig. 8b can be attributed to the substantial contribution of the molecular interference at mass 136. The magnitude of the deviations from the true ratios (Fig. 8c) are, however, also dependent on the intrinsic Ba concentrations. This is most likely the reason why molecular interferences, apparently, do not affect the Ba isotopic compositions obtained for the KJB fraction, which has a relatively high Ba abundance (380 µg/g) compared with the large SiC grains analyzed here (Table 2).

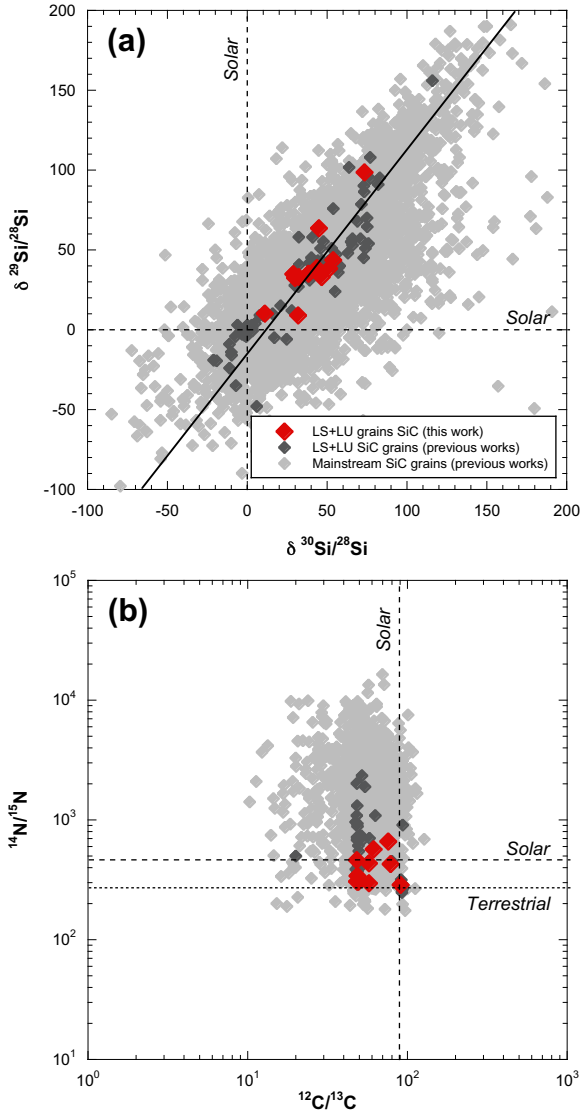

Fig. 7. Silicon-, C-, and N-isotopic ratios of stardust SiC grains from the LS + LU fractions analyzed in the present study. Data for large LS + LU SiC grains and small mainstream SiC grains from previous analyses (Hynes and Gyngard, 2009) are shown for comparison. Error bars from previous measurements are omitted for clarity. Black dashed lines indicate the solar ratios ($^{14}N/^{15}N$ ratio according to Marty et al., 2011). The terrestrial $^{14}N/^{15}N$ ratio is also indicated in the figure by a black dotted line. (a) Si-isotopic ratios expressed as deviations from the solar ratios in parts per 1000 (δ-values). Also shown is the so-called mainstream correlation line as solid line, with a slope of 1.35 (Zinner et al., 2006). (b) $^{14}N/^{15}N$ ratios plotted against $^{12}C/^{13}C$ ratios. Error bars (1σ) are smaller than the symbols.

We must highlight the surprising coincidence that stardust SiC grains, which are clearly affected by mass interferences, have Ba isotopic patterns that are similar to the *s*-process Ba pattern predicted for the AGB stellar envelope (Fig. 8b). The same feature can be observed for the synthetic "pure" SiC standard (Fig. 8a). This is apparently just

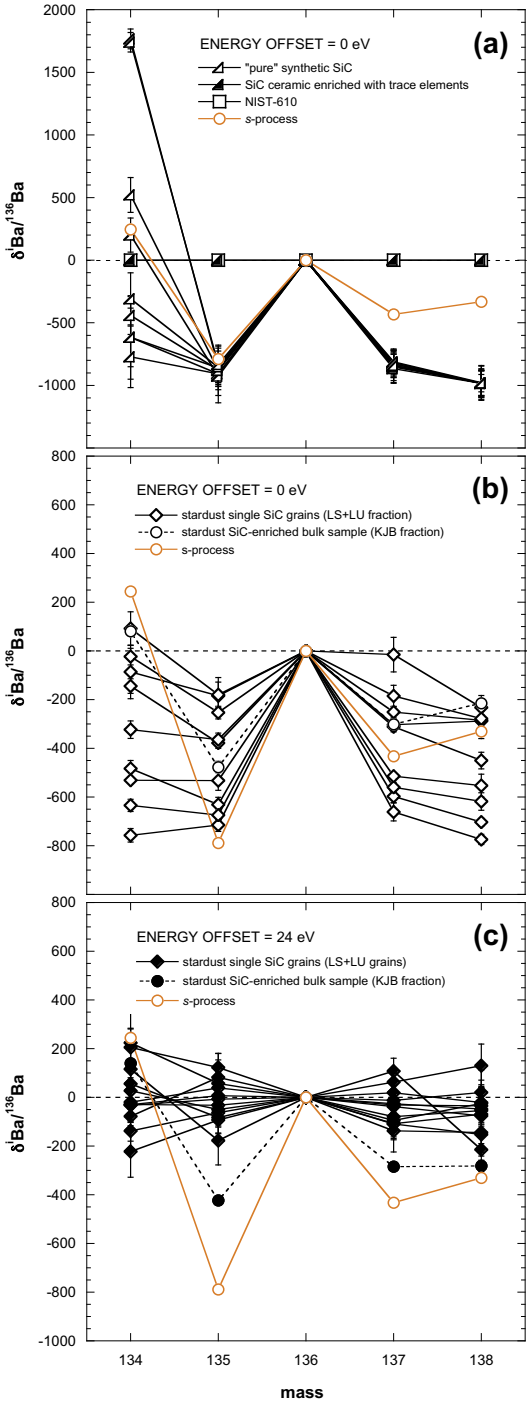

Fig. 8. Barium isotopic patterns normalized to ^{136}Ba and expressed as deviations from the solar isotopic ratios in permil (δ-values). (a) Uncorrected Ba isotopic compositions determined for the NIST-610 glass, the SiC ceramic enriched with trace elements, and a "pure" synthetic SiC measured in the course of an analytical session with an energy offset of 0 eV; ratios for the "pure" synthetic SiC are apparently those between molecular interferences at the Ba isotope mass positions. Stardust SiC single grain data obtained with an energy offset of 0 eV (b) and 24 eV (c). Error bars are 1σ. The *s*-process prediction for the AGB stellar envelope after the last TP with TDU (11th) of a 2 $M_{\odot}$ AGB star of solar metallicity reported by Cristallo et al. (2009) is also shown for comparison.

a coincidence, but it raises the question of whether the mass interferences observed here have also compromised previous ion microprobe Ba-isotope determinations without energy filtering in stardust SiC grains.

Barium isotopic compositions have previously been measured in stardust SiC aggregates (Ott and Begemann, 1990; Zinner et al., 1991; Prombo et al., 1993; Yin et al., 2006) and single grains (Savina et al., 2003; Barzyk et al., 2007; Marhas et al., 2007). Only the measurements of Zinner et al. (1991) and Marhas et al. (2007) were carried out with the ion microprobe. In Fig. 9 we present the Ba isotopic data obtained for single stardust SiC grains in three-isotope plots. For comparison, we have also included data obtained by Savina et al. (2003), Barzyk et al. (2007) and Marhas et al. (2007). The data reported by both Savina et al. (2003) and Barzyk et al. (2007) were obtained by RIMS, which strongly suppresses interferences from atoms of other not-resonantly-ionized elements and molecules (e.g., Nicolussi et al., 1998a). All single grains shown in Fig. 9 are classified as "mainstream grains" based on their C-, N-, and Si-isotopic compositions. The primary difference between the Ba isotopic results reported here and those obtained by Savina et al. (2003), Barzyk et al. (2007), and Marhas et al. (2007) is the much narrower distribution of our data on three-isotope plots, with all grains (measured with an energy offset of 24 eV) lying close to the solar Ba isotopic compositions. Whereas the Savina et al. (2003) and Barzyk et al. (2007) data were obtained with RIMS and, therefore, did not suffer with potential interferences with molecular ions, the Marhas et al. (2007) data were obtained with SIMS without any energy filtering. It is thus possible that molecular interferences affected these data. On the other hand, most of the grains analyzed by Marhas et al. (2007) had much higher Ba contents than the LS + LU grains analyzed in the present study, and interferences by molecular ions probably played a smaller role. This is indicated by the fact that most of the Marhas et al. (2007) data overlap with the Barzyk et al. (2007) data (Fig. 9).

Marhas et al. (2007) reported that some stardust SiC grains showed large apparent excesses in $^{134}Ba^{+}$, which were attributed to the presence of CsH^{+} interference, as the grains had been previously bombarded with Cs^{+}. Nineteen out of the 26 mainstream SiC grains analyzed by Marhas et al. (2007) have Cs concentrations ranging from 0.3 to 137 μg/g; Cs concentrations higher than 468 μg/g were found for seven mainstream grains (note that the concentrations reported by Marhas et al. were calculated using NIST-611 silicate glass as a normalization standard). These authors also reported that CsH_x interferences were present on other Ba isotopes and that a Cs correction was applied to the isotopic ratios. However, as stated in Section 2.4, neither the mass scans shown in Fig. 3 nor the Ba isotopic ratios obtained from the NIST-610 glass show contributions from CsH interferences. In addition, the high-resolution spectrum of the mass region around ^{133}Cs obtained from the SiC ceramic and the "pure" synthetic SiC has shown the presence of molecular interferences (Fig. 5). Consequently, corrections of the Ba isotopic ratios based on measurements of ^{133}Cs peak are not straightforward and can be misleading.

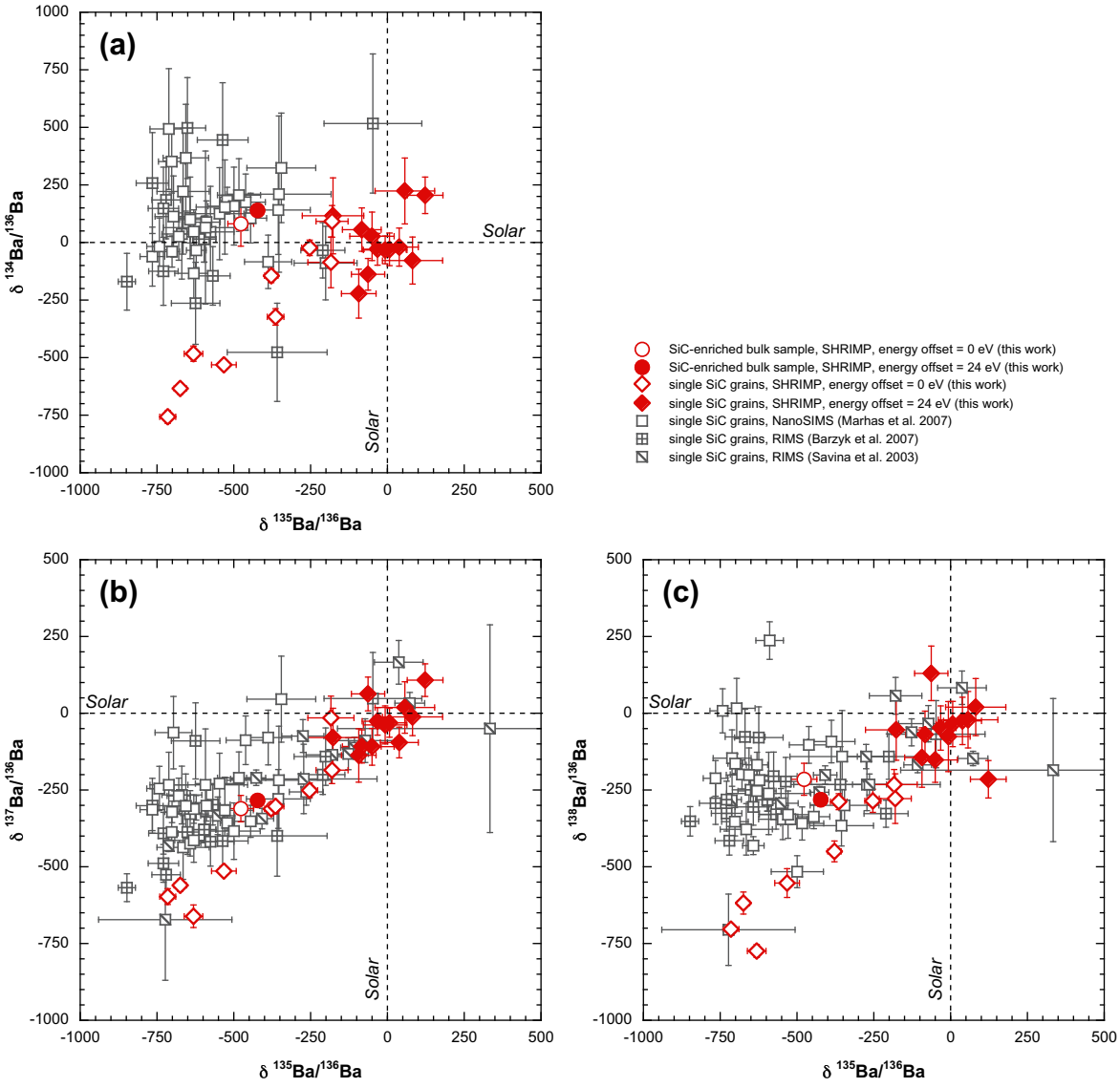

Fig. 9. Barium three-isotope δ-value plots of stardust SiC grains. (a) $\delta^{134}Ba/^{136}Ba$ versus $\delta^{135}Ba/^{136}Ba$, (b) $\delta^{137}Ba/^{136}Ba$ versus $\delta^{135}Ba/^{136}Ba$, and (c) $\delta^{138}Ba/^{136}Ba$ versus $\delta^{135}Ba/^{136}Ba$. Single grain data from Savina et al. (2003), Barzyk et al. (2007) and Marhas et al. (2007) are shown for comparison. Error bars are 1σ. ^{134}Ba was not reported by Savina et al. (2003).

We should point out, however, that we analyzed stardust SiC grains that are much larger than the ones analyzed by Marhas et al. (2007). Marhas and co-workers studied grains with sizes between 0.2 and 2.6 μm, whereas we studied grains with sizes between 7 and 58 μm. These large SiC grains are known for having comparatively low trace element abundances (Virag et al., 1992; Gyngard et al., 2009b), which in principle make them more susceptible to contributions from molecular interferences and also from contamination with isotopically normal material.

The fact that the stardust SiC grains analyzed here display Ba isotopic compositions close to normal, despite likely having been formed in the outflows of low mass carbon-rich AGB stars with close-to-solar metallicity, is interesting. Contamination with terrestrial or meteoritic Ba is a possibility. However, in order to minimize any potential surface contamination, the primary beam was rastered across an area slightly larger than the analytical spot for ~60 s before data acquisition. If contamination is carried primarily on the surface, one would expect a depth dependence of the contamination revealed as the grain surface is slowly sputtered away. Based on the behavior of the isotopic ratios and the Ba ion signals as a function of acquisition time, there is no evidence from our analyses to suggest that the Ba isotopic compositions are not intrinsic to the grains or result from surface contamination. Furthermore, we also periodically monitored the Au-foil substrate where the grains were deposited and no Ba counts were detected.

4. DISCUSSION

Previous studies on size-separated SiC fractions from the Murchison meteorite have shown that several isotopic and abundance properties vary with grain size. Small SiC grains have notably higher trace-element abundances than larger SiC grains (e.g., Amari et al., 1995). Noble-gas studies indicate an increase of $^{86}Kr/^{82}Kr$ ratios and ^{22}Ne–G abundances with increasing grain size (Lewis et al., 1994). Isotopic compositions of heavy elements also show evidence of a grain-size dependence (Zinner et al., 1991; Prombo et al., 1993; Savina et al., 2003; Podosek et al., 2004). This is especially true for Ba-isotopic ratios. Both Zinner et al. (1991) and Prombo et al. (1993) found that $^{138}Ba/^{136}Ba$ ratios measured in SiC-rich bulk samples decrease with increasing grain size. This trend is, however, not apparent for recent Ba studies on single SiC grains (Savina et al., 2003; Barzyk et al., 2007; Marhas et al., 2007; this work), although a grain-size dependence is observed for $^{135}Ba/^{136}Ba$ ratios on single SiC measurements, with larger grains showing higher $^{135}Ba/^{136}Ba$ ratios than smaller grains.

The new data presented here for LS + LU grains are consistent with previous observations that the degree of Ba isotopic anomaly varies with grain size (Fig. 10; see also Fig. 5 in Savina et al., 2003). Marhas et al. (2007) suggested that the SiC grains for which data are reported by Savina et al. (2003), which show less extreme (i.e., closer to solar) Ba isotopic ratios compared to the SiC data reported by Marhas et al. (2007), were contaminated with solar Ba. However, we note that the Ba-isotopic ratios reported by Savina et al. (2003) for grains from the KJG fraction (grain size between 2.5 and 5.3 μm), whose sizes lie between those of the grains measured by Marhas et al. (2007) and those reported here, are consistent with the observation that Ba ratios (mainly $\delta^{135}Ba/^{136}Ba$ and, to a lesser extent, $\delta^{137}Ba/^{136}Ba$) are dependent on grain size. Although data obtained for many fractions of SiC-enriched bulk samples extracted from the Murchison meteorite (KJB, KJC, KJD, KJE, KJF; Zinner et al., 1991; Prombo et al., 1993) are also consistent with this observation, the results obtained by Barzyk et al. (2007) for grains from the KJH fraction (grain size between 3.4 and 5.9 μm) do not follow this trend. These grains are larger than those measured by Savina et al. (2003) and have, on average, larger Ba anomalies than grains from the KJG fraction (Fig. 10). Measurements with better precision on grains from a wide range of sizes are needed in order to confirm the grain-size dependency of Ba isotopic ratios.

It should also be noted that the grains from the LS + LU fractions contain a unique feature not observed in the small grain population. The LS + LU grains can be grouped into two morphologically distinct classes: one with anhedral blocky characteristics, where most grains appear to have flat and smooth surfaces, and the other with euhedral features similar to those observed in smaller grains (Virag et al., 1992). Anhedral grains are dominant among grains with sizes >10 μm. In addition, while most of the anhedral grains lack evidence for the presence of ^{26}Al (Virag et al., 1992), preliminary data on euhedral grains show evidence of ^{26}Al. One of the most remarkable features of LS + LU grains, the clustering of C, Si, and Ti isotopic compositions (Ireland et al., 1991; Virag et al., 1992), is noticeably more prominent among anhedral grains. Although these observations indicate that some isotopic properties are also dependent on the morphology of the grains, we see no clear distinction for Ba-isotopic ratios between large euhedral and anhedral grains (Fig. 10).

Since the isotopic signatures of stardust grains reflect the interplay between neutron density, temperature, neutron exposure, and mixing events operating in stars, the grain-size dependency of some isotopic ratios may, therefore, indicate that the grain size is also governed by the same factors that control the isotopic compositions of stardust SiC grains, ultimately, being the stellar mass, metallicity, and stage of stellar evolution.

Next, we compare the available Ba data with *s*-process model predictions for the envelope compositions of low-mass AGB stars. These predictions involve the mixing between two components, one close to the solar composition, representing the initial composition of the stellar envelope (in stardust studies this is traditionally referred to as the N-component), and the other with isotopic characteristics close to those predicted for pure *s*-process (the G-component) (e.g., Zinner et al., 1991; Nicolussi et al., 1997; Savina et al., 2004). The magnitude of the departure from the N-component towards the G-component depends on the efficiency and the number of mixing episodes, also known as third dredge-up(s) (TDU), which occur when the convective envelope penetrates into the He intershell. The TDU causes newly synthesized ^{12}C and *s*-processed material to be mixed into the convective envelope of the star (e.g., Lugaro et al., 2003). As the mixing episodes proceed, the AGB stellar envelope becomes progressively enriched in carbon and *s*-process elements.

In Fig. 11 the single grain Ba data are compared to the *s*-process AGB predictions from the FRUITY database (Cristallo et al., 2009, 2011), which were computed using the FRANEC stellar evolution and nucleosynthesis code. The models have been selected to reach C/O > 1 in the envelope so that the condition for the formation of SiC is satisfied, and they all show large Ba isotopic deviations from solar compositions (Fig. 11 and Table 3). We also present a model computed with the Monash nucleosynthesis code (e.g., Lugaro et al., 2012) based on the evolutionary sequence of the 1.25 $M_{\odot}$ model presented by Karakas et al. (2010). This model was computed with the Mt. Stromlo stellar evolution code and some overshoot was introduced, resulting in three TDU episodes, and the star becoming C rich for the last two, with C/O = 1.2 and 2.2, respectively. The Ba isotopic composition in the envelope of this star when it reaches C/O > 1 for the first time is close to the solar composition (Fig. 11 and Table 3), in good agreement with the observed Ba isotopic ratios in large SiC grains from the LS + LU fractions. One possible reason that the grains could condense in the envelope after the second TDU (according to the predictions from 1.25 $M_{\odot}$ model) but not after the third is that after the third TDU the C/O ratio is too high (C/O = 2.2) and one would expect to condense graphite and not SiC.

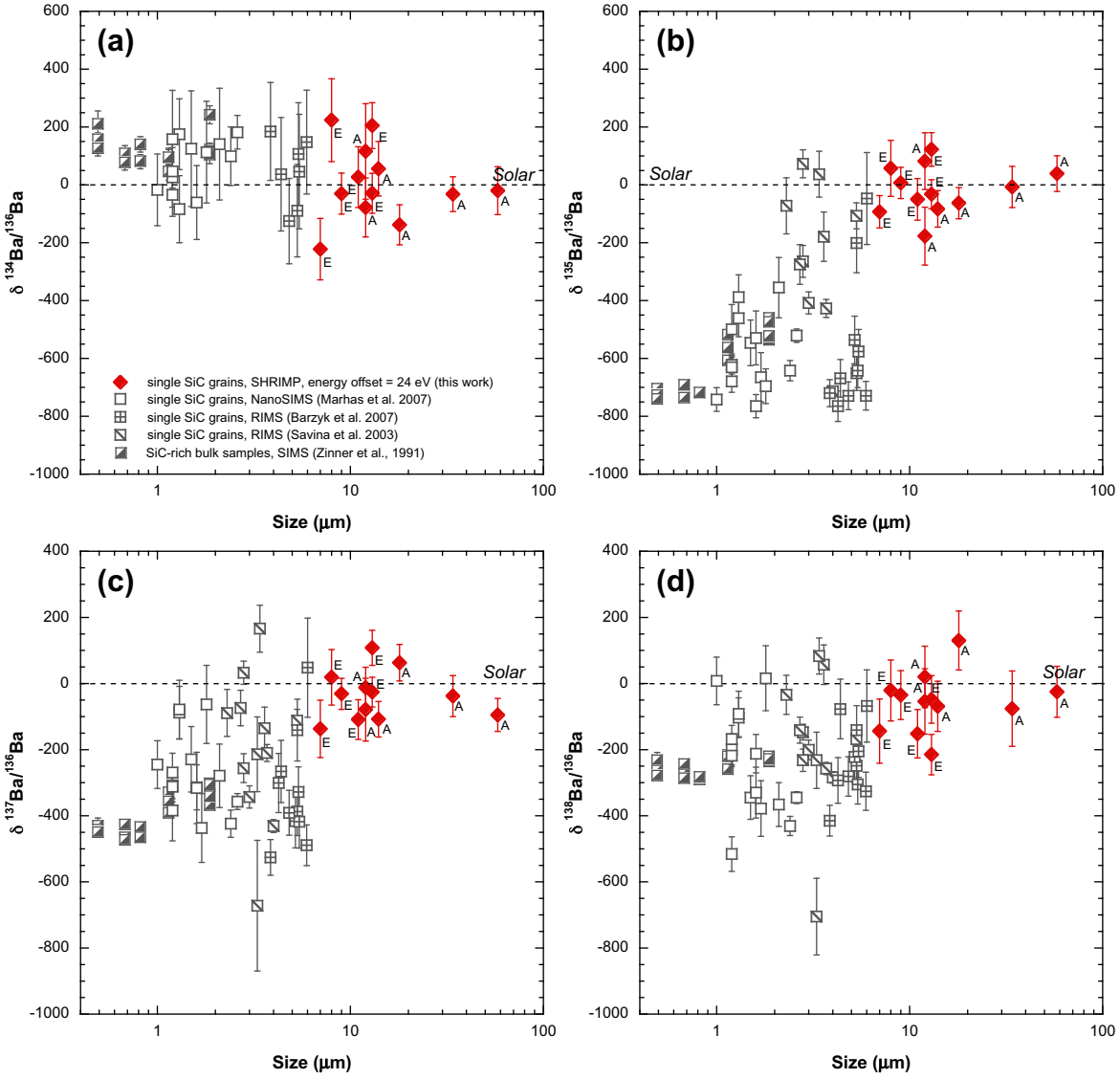

Fig. 10. Barium isotopic compositions, (a) $\delta^{134}Ba/^{136}Ba$, (b) $\delta^{135}Ba/^{136}Ba$, (c) $\delta^{137}Ba/^{136}Ba$, and (d) $\delta^{138}Ba/^{136}Ba$, versus grain size for stardust SiC grains. The grain sizes for the LS + LU grains (this work) correspond to the grain's longer axis as measured by SEM. Error bars are 1σ. Literature data points with errors larger than 200‰ are not plotted. Morphologies of SiC grains from the LS + LU fractions after Virag et al. (1992): A = anhedral, blocky, smooth surfaces and E = round to irregular, euhedral features, bounded by one or more crystal faces.

In our 1.25 $M_{\odot}$ model, the ^{13}C in the ^{13}C pocket does not completely burn radiatively in the interpulse period, but some of it is left over and ingested in the following thermal pulses (TP), where it burns under convective conditions, resulting in lower neutron fluences. The ^{22}Ne neutron source is never activated, as the temperature in the thermal pulses is always below 2.7×10^8 K. When ^{13}C burns convectively rather than radiatively, the *s*-process efficiency is strongly reduced because (i) the neutrons are released over a region at least an order of magnitude more extended in mass and (ii) the abundance of the ^{14}N nucleus, a strong neutron poison via the $^{14}N(n,p)^{14}C$ reaction, is ~5 times higher. Higher neutron fluences (i.e., TPs) are needed to build up the *s*-process elements, which results in a decoupling of the surface abundances of *s*-process elements from the C abundance during the early TDU episodes. This *s*-process model should be considered as preliminary because it does not include the branching points at the Cs isotopes, however, it is presented here as an example of the possibility that a low-mass AGB model can predict a C-rich envelope characterized by essentially solar Ba isotopic ratios.

In this context, the isotopically close-to-normal Ba observed in large SiC grains from the LS + LU fractions suggests that conditions for growth of large SiC are more favorable in very low-mass AGB stars and during the early C-rich stages of AGB evolution before many dredge-up episodes have happened. This hypothesis is supported by the

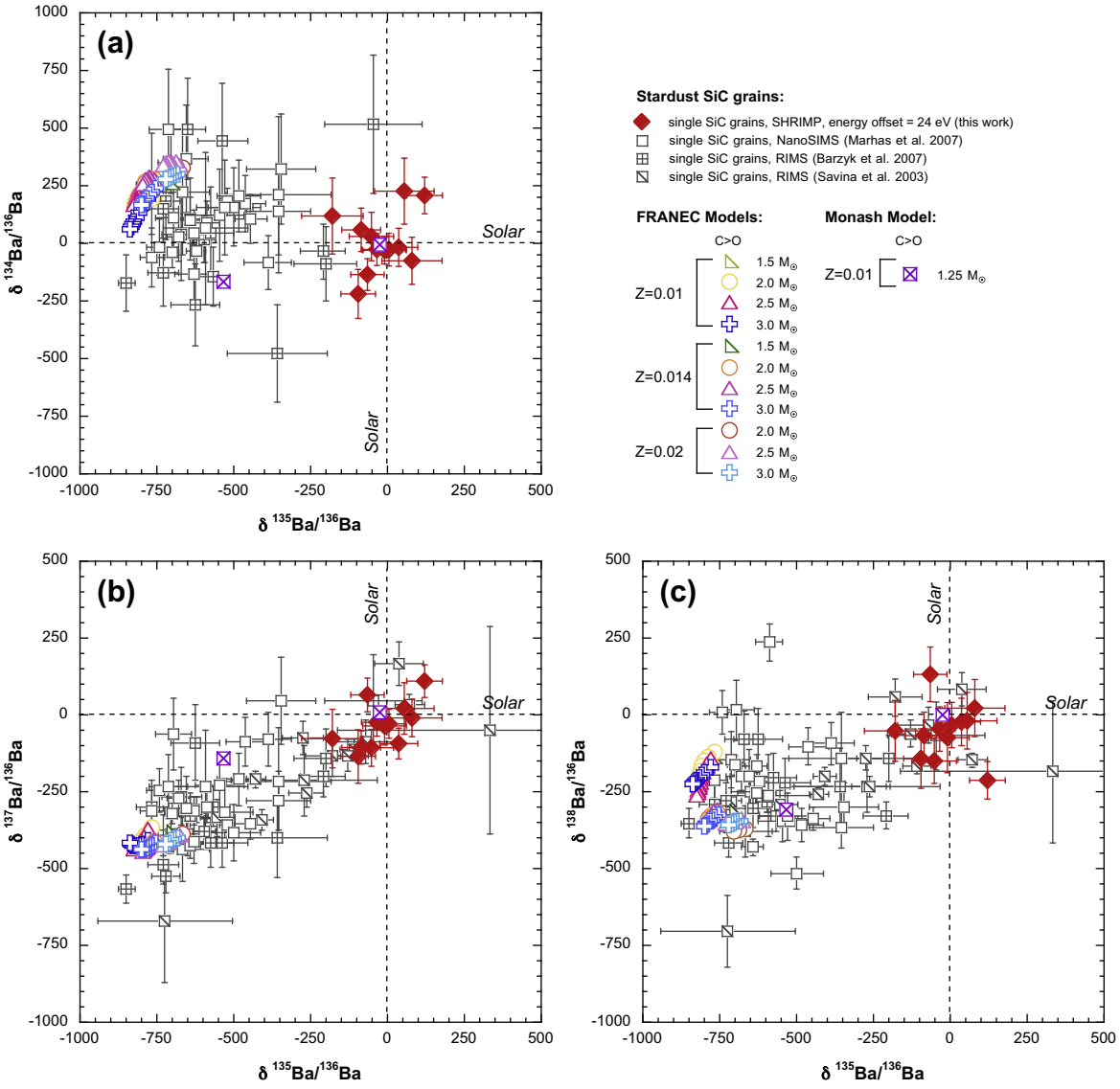

Fig. 11. Barium three-isotope plots normalized to solar for stardust SiC grains. (a) $\delta^{134}Ba/^{136}Ba$ versus $\delta^{135}Ba/^{136}Ba$, (b) $\delta^{137}Ba/^{136}Ba$ versus $\delta^{135}Ba/^{136}Ba$, and (c) $\delta^{138}Ba/^{136}Ba$ versus $\delta^{135}Ba/^{136}Ba$. SiC data are compared with *s*-process model predictions (FRANEC and Monash models) for the envelope compositions of low-mass AGB stars of different masses and metallicities (see text for details). Symbols are only shown when the C/O in the stellar envelope reaches values higher than 1. Shifts in the isotopic ratios for a given model are the result of the trajectory of envelope isotopic compositions after successive TDU episodes. Single grain data from Savina et al. (2003), Barzyk et al. (2007) and Marhas et al. (2007) are also shown.

observations made by Speck et al. (2005), which showed that the evolutionary sequence in carbon star spectra is consistent with a grain size evolution, such that grains formed in stellar outflows of AGB stars become progressively smaller as the star evolves. The match between the SiC data and the predictions from the 1.25 $M_\odot$ model also supports the view that stardust grains can only grow to relatively large sizes in the stellar atmosphere of the lowest mass AGB stars (Nuth et al., 2006) where a perfect balance between radiation pressure and stellar gravity, needed to promote long-term stable growth of large grains, can be achieved.

It should be noted that the decoupling of the *s*-process and the C surface abundances could be achieved in any AGB model by artificially decreasing the mass of the ^{13}C pocket or the efficiency of the ^{13}C neutron source, as has been done for example by Lugaro et al. (2003). In our 1.25 $M_\odot$ model, instead, the decoupling is derived self-consistently due to the effect of ^{13}C burning convectively in stars of mass lower than ~1.5 $M_\odot$. Whichever way it is achieved, this decoupling depends on the uncertainties related to the modeling of the mixing between the envelope and the He intershell, which affects not only the formation of the ^{13}C pocket, but also the TDU efficiency. In fact, as mentioned above, our 1.25 $M_\odot$ model experiences enough TDU to become C rich only when some overshoot is applied at the base of the convective envelope (as discussed in Karakas et al., 2010).

Table 3
Barium isotopic compositions (shown as δ-values) in the stellar envelope obtained from the FRANEC and Monash models.

Z	Mass	TDU episodes[a]	TDU with C/O > 1[b]	$\delta^{134}Ba/^{136}Ba$ at C/O = 1[c]	$\delta^{134}Ba/^{136}Ba$ Final[d]	$\delta^{135}Ba/^{136}Ba$ at C/O = 1[c]	$\delta^{135}Ba/^{136}Ba$ Final[d]	$\delta^{137}Ba/^{136}Ba$ at C/O = 1[c]	$\delta^{137}Ba/^{136}Ba$ Final[d]	$\delta^{138}Ba/^{136}Ba$ at C/O = 1[c]	$\delta^{138}Ba/^{136}Ba$ Final[d]
FRANEC models											
0.01	1.5	7	4	199	229	−770	−798	−382	−414	−139	−155
	2.0	12	8	194	169	−798	−822	−368	−434	−122	−214
	2.5	18	13	239	166	−780	−824	−372	−438	−143	−263
	3.0	15	9	193	62	−778	−838	−410	−418	−171	−226
0.014	1.5	5	1	262	262	−704	−704	−378	−378	−312	−312
	2.0	11	5	280	264	−760	−787	−413	−437	−315	−341
	2.5	16	10	279	254	−758	−796	−405	−446	−310	−352
	3.0	14	7	239	165	−755	−800	−418	−439	−325	−363
0.02	2.0	10	4	328	333	−665	−702	−387	−412	−370	−381
	2.5	16	8	341	341	−673	−731	−391	−425	−344	−355
	3.0	14	5	298	278	−685	−719	−399	−419	−345	−358
Monash model											
0.01	1.25	3	2	−4	−168	−24	−533	10	−140	1	−308

[a] Total number of TDU episodes experienced by the AGB star.
[b] Number of TDU episodes at which the C/O ratio in the stellar envelope becomes higher than unity.
[c] Ba isotopic compositions in the stellar envelope at the time the C/O ratio reaches unity.
[d] Ba isotopic compositions in the stellar envelope after the last TDU.

A third possibility to achieve the decoupling of C and the *s*-process elements is to cut short the AGB evolution, for example, via binary interaction. After the first TDU episode an AGB star (depending on its envelope mass and the efficiency of the TDU) could become C rich, but not *s*-process rich, because the formation of the first ^{13}C pocket occurs after this first TDU episode, which means that at least two TDU episodes are needed to carry the *s*-process elements to the stellar surface. Though this solution appears somewhat forced, it may find some support in the observation that large dust grains grow more likely in stable circumbinary disks, where material lost by AGB stars can reside for a relatively long time (e.g., Jura, 1997).

A puzzling Ba isotopic signature is found in Grain WU-19. This grain shows enhancements in ^{135}Ba and ^{137}Ba, a possible signature of the *rapid* neutron-capture process (*r*-process), but a typical *s*-process signature in the $^{134}Ba/^{136}Ba$ and $^{138}Ba/^{136}Ba$ ratios. If the *r*-process signature was initially present in the star, it would have been erased by the following *s*-process. It thus appears that the *r*-process signature has been added to the gas after the *s*-process signature had been established. This is an unusual occurrence, which may point to effects related to the presence of a nearby *r*-process source, e.g., a binary companion.

If we assume that stellar parameters, such as mass, metallicity, and stage of stellar evolution, were indeed responsible for the size and isotopic compositions of stardust SiC grains, other isotopic systems should also show a size trend similar to the one observed for Ba isotopes. Measurements of heavy elements, however, have been scarce, and when available, are limited to one size fraction (e.g., Zr, KJH fraction, Nicolussi et al. (1997) and Barzyk et al. (2007); Mo, KJH fraction, Nicolussi et al. (1998a) and Barzyk et al. (2007); Ru, KJG fraction, Savina et al. (2004)). An exception is Sr, for which different size fractions have been measured (KJG fraction, Nicolussi et al., 1998b; KJB, KJC, KJD, and KJE fractions, Podosek et al., 2004). A grain-size dependence is observed for the $^{88}Sr/^{86}Sr$ ratio on the SiC-rich bulk samples measured by Podosek et al. (2004), in which the coarser fractions have lower $^{88}Sr/^{86}Sr$ ratios. Unfortunately, no Sr measurements have been made on SiC grains larger than 5 μm. The 1.25 $M_\odot$ model predicts that SiC grains should have smaller than solar $^{88}Sr/^{86}Sr$ ratios. Strontium isotopic measurements in the same grains analyzed here would be extremely helpful, shedding light on the most likely stellar progenitors of large SiC grains.

Another possibility that needs to be considered is that the close-to-solar Ba isotopic ratios of large stardust SiC grains from the LS + LU fractions are the result of contamination with solar Ba. There is a potential problem of contamination with foreign materials and minerals, originating either from the meteorite itself or as a result of sample preparation. These large SiC grains have comparatively low trace element abundances, which in principle make them more susceptible to contributions from molecular interferences and also from contamination with isotopically normal material. Previous Ba studies on single SiC grains have identified grains contaminated with Ba by performing silicon–barium ion imaging (Marhas et al., 2007) or by multiple-element analyses (Barzyk et al., 2007). Unfortunately, SHRIMP-RG does not have the capabilities of ion imaging present in the NanoSIMS. However, multiple-element analyses can be performed. Preliminary data on Pb isotopes in the same grains analyzed for Ba also mostly show close-to-solar (=primordial) Pb isotopic ratios. Both isotopic systems in 6 grains out of 8 are in agreement with predictions from the 1.25 $M_\odot$ AGB model.

A final point that must be highlighted is the mechanism of incorporation of Ba into SiC grains. Two scenarios have been proposed to explain incorporation of trace elements into stardust SiC grains: (a) condensation as solid solution (Amari et al., 1995; Lodders and Fegley, 1995), which will depend on C/O ratio, pressure, volatility and crystal structure; and (b) ion implantation, which will depend on the ionization potential of the respective element (Verchovsky et al., 2004). Ion implanted is the favored mechanism for introducing noble gases into stardust SiC grains (Lewis et al., 1990; Verchovsky et al., 2004). The correlation observed between grain-size and Ba abundance, with small grains having higher Ba abundances, have led some investigators to propose that Ba is indeed implanted into SiC grains (e.g., Verchovsky et al., 2004; Marhas et al., 2007). Verchovsky et al. (2004) suggested that a fraction of alkaline-earth elements (e.g., Ba and Sr) have been implanted into SiC grains during the main stage of AGB evolution, however the proportion of implanted ions approach zero for large grains, like the ones analyzed in the present study.

5. CONCLUSIONS

Barium isotopes have previously been measured in stardust SiC grains by a number of different analytical techniques. SHRIMP-RG analyses of silicate and carbide reference materials presented in this study revealed several molecular interferences, particularly on ^{134}Ba and ^{136}Ba. We have shown that these interferences can only be suppressed by a combination of high-mass resolution and energy filtering and that, consequently, previous ion microprobe determinations where this approach was not taken need to be interpreted cautiously. A comparison between Ba isotopic ratios determined on single stardust SiC grains with a range of sizes revealed a correlation between isotopic anomalies and grain size, with larger grains typically being less anomalous.

Although we cannot completely rule out that the close-to-solar Ba isotopic ratios in the LS + LU grains are due to contamination, our data are consistent with observations from previous studies that point to the existence of a relationship between stardust SiC grain size, trace-element abundances, and the magnitude of isotopic deviations from solar compositions. Such a relationship suggests that stellar parameters such as mass, metallicity, and stage of stellar evolution may control not only the abundance and isotopic signature of *s*-process elements, but also the kinetics of grain growth. In this context, the Ba isotopic measurements reported here for large SiC grains from the LS + LU fractions are consistent with grain condensation in the envelope of very low-mass AGB stars (1.25 $M_\odot$) with close-to-solar metallicity. This hypothesis expresses the idea that stardust

grains can only grow to relatively large sizes in the stellar atmosphere of the lowest-mass AGB stars. We suggest that large SiC grains may have grown during the early C-rich stages of the evolution of low-mass AGB stars or in stable structures around AGB stars whose evolution was cut short due to binary interaction, before the AGB envelope had already been largely enriched with the products of *s*-process nucleosynthesis. Further isotopic measurements in large SiC grains are needed to test this idea.

ACKNOWLEDGMENTS

We thank Torsten Henkel, Andrew Davis, an anonymous reviewer, and AE Sara Russell for their comments, which helped to improve the manuscript. We are grateful to Roy Lewis for providing the LS + LU grains, to Antti Kallio for helping with the identification of molecular interferences, and to Sergio Cristallo, Amanda Karakas, and Joelene Buntain for sharing their stellar *s*-process models. J.N. Ávila acknowledges support by CNPq Grants 200081/2005-5 and 500798/2011-7. She thanks the Australian National University for an ANU Vice-Chancellor's Higher Degree Research Travel Grant. T.R. Ireland acknowledges support by ARC Grants DP0342772 and DP0666751. E. Zinner acknowledges support by NASA Grants NNX08AG71G and NNX11AH14G. G. Mallmann acknowledges support by FAPESP Grant 2010/05512-1. M. Lugaro acknowledges the support of the ARC via a Future Fellowship and of Monash University via a Monash fellowship.

REFERENCES

Amari S., Lewis R. S. and Anders E. (1994) Interstellar grains in meteorites. I. Isolation of SiC, graphite, and diamond; size distributions of SiC and graphite. *Geochim. Cosmochim. Acta* **58**, 459–470.

Amari S., Hoppe P., Zinner E. and Lewis R. S. (1995) Trace-element concentrations in single circumstellar silicon carbide grains from the Murchison meteorite. *Meteorit. Planet. Sci.* **30**, 679–693.

Amari S., Zinner E. and Lewis R. S. (2000) Isotopic compositions of different presolar silicon carbide size fractions from the Murchison meteorite. *Meteorit. Planet. Sci.* **35**, 997–1014.

Ávila J. N., Lugaro M., Ireland T. R., Gyngard F., Zinner E., Cristallo S., Holden P., Buntain J., Amari S. and Karakas A. (2012) Tungsten isotopic compositions in stardust SiC grains from the Murchison meteorite: constraints on the *s*-process in the Hf-Ta-W-Re-Os region. *Astrophys. J.* **744**, 49 (13pp).

Ávila J. N., Ireland T. R., Lugaro M., Gyngard F., Zinner E., Cristallo S., Holden P. and Rauscher T. (2013) Europium s-process signature at close-to-solar metallicity in stardust SiC grains from Asymptotic Giant Branch stars. *Astrophys. J. Lett.* **768**, L18 (7pp).

Barzyk J. G., Savina M. R., Davis A. M., Gallino R., Gyngard F., Amari S., Zinner E., Pellin M. J., Lewis R. S. and Clayton R. N. (2007) Constraining the ^{13}C neutron source in AGB stars through isotopic analysis of trace elements in presolar SiC. *Meteorit. Planet. Sci.* **42**, 1103–1119.

Bernatowicz T. J., Messenger S., Pravdivtseva O., Swan P. and Walker R. M. (2003) Pristine presolar silicon carbide. *Geochim. Cosmochim. Acta* **67**, 4679–4691.

Cerrigone L., Hora J. L., Umana G. and Trigilio C. (2009) SPITZER detection of polycyclic aromatic hydrocarbons and silicate features in post-AGB stars and young planetary nebulae. *Astrophys. J.* **703**, 585–600.

Cristallo S., Straniero O., Gallino R., Piersanti L., Domínguez I. and Lederer M. T. (2009) Evolution, nucleosynthesis, and yields of low-mass asymptotic giant branch stars at different metallicities. *Astrophys. J.* **696**, 797–820.

Cristallo S., Piersanti L., Straniero O., Gallino R., Domínguez I., Abia C., Di Rico G., Quintini M. and Bisterzo S. (2011) Evolution, nucleosynthesis, and yields of low-mass asymptotic giant branch stars at different metallicities. II. The FRUITY database. *Astrophys. J. Suppl. Ser.* **197**, 17 (21pp).

Dodson M. H. (1978) A linear method for second-degree interpolation in cyclical data collection. *J. Phys. E* **11**, 296.

Eggins S. M., Kinsley L. P. J. and Shelley J. M. G. (1998) Deposition and element fractionation processes during atmospheric pressure laser sampling for analysis by ICP-MS. *Appl. Surf. Sci.* **127**, 278–286.

Fahey A. (1998) Details of the measurement of rare earth and other trace element abundances by secondary ion mass spectrometry. *Int. J. Mass Spectrom.* **176**, 63–76.

Gielen C., Bouwman J., Van Winckel H., Loyd Evans T., Woods P. M., Kemper F., Marengo M., Meixner M., Sloan G. C. and Tielens G. G. M. (2011) Silicate features in Galactic and extragalactic post-AGB disks. *Astron. Astrophys.* **533**, A99.

Gyngard F., Amari S., Zinner E. and Ott U. (2009a) Cosmic-ray exposure ages of large presolar SiC grains. *Publ. Astron. Soc. Australia* **26**, 278–283.

Gyngard F., Amari S., Zinner E. and Ott U. (2009b) Interstellar exposure ages of large presolar SiC grains from the Murchison meteorite. *Astrophys. J.* **694**, 359–366.

Heck P., Gyngard F., Ott U., Meier M. M. M., Ávila J. N., Amari S., Zinner E., Lewis R. S., Baur H. and Wieler R. (2009) Interstellar residence times of presolar SiC dust grains from the Murchison carbonaceous meteorite. *Astrophys. J.* **698**, 1155–1164.

Hoppe P., Amari S., Zinner E., Ireland T. and Lewis R. S. (1994) Carbon, nitrogen, magnesium, silicon, and titanium isotopic compositions of single interstellar silicon carbide grains from the Murchison carbonaceous chondrite. *Astrophys. J.* **430**, 870–890.

Hynes K. M. and Gyngard F. (2009) The presolar grain database: http://presolar.wustl.edu/~pgd. *Lunar Planet. Sci. XL.* #1198 (abstr.).

Ireland T. R., Zinner E. and Amari S. (1991) Isotopically anomalous Ti in presolar SiC from the Murchison meteorite. *Astrophys. J.* **376**, L53–L56.

Jura M. (1997) Disks around post-main sequence binaries. *Astrophys. Space Sci.* **251**, 81–88.

Karakas A. I., Campbell S. W. and Stancliffe R. J. (2010) Is extra mixing really needed in asymptotic giant branch stars? *Astrophys. J.* **713**, 374–382.

Lewis R., Amari S. and Anders E. (1990) Meteoritic silicon carbide: pristine material from carbon stars. *Nature* **348**, 293–298.

Lewis R., Amari S. and Anders E. (1994) Interstellar grains in meteorites. II. SiC and its noble gases. *Geochim. Cosmochim. Acta* **58**, 471–494.

Lodders K. and Fegley B. (1995) The origin of circumstellar silicon carbide grains found in meteorites. *Meteorit. Planet. Sci.* **30**, 661–678.

Lugaro M., Davis A. M., Gallino R., Pellin M. J., Straniero O. and Kappeler F. (2003) Isotopic compositions of strontium, zirconium, molybdenum, and barium in single presolar SiC grains and asymptotic giant branch stars. *Astrophys. J.* **593**, 486–508.

Lugaro M., Karakas A. I., Stancliffe R. J. and Rijs C. (2012) The *s*-process in asymptotic giant branch stars of low metallicity and the composition of carbon-enhanced metal-poor stars. *Astrophys. J.* **742**, 2 (18pp).

Marhas K. K., Hoppe P. and Ott U. (2007) NanoSIMS studies of Ba isotopic compositions in single presolar silicon carbide grains from AGB stars and supernovae. *Meteorit. Planet. Sci.* **42**, 1077–1101.

Marty B., Chaussidon M., Wiens R. C., Jurewicz A. J. G. and Burnett D. S. (2011) A ^{15}N-poor isotopic composition for the Solar System as shown by Genesis Solar Wind samples. *Science* **332**, 1533–1536.

Nicolussi G. K., Davis A. M., Pellin M. J., Lewis R. S., Clayton R. N. and Amari S. (1997) *s*-Process zirconium in presolar silicon carbide grains. *Science* **277**, 1281–1284.

Nicolussi G. K., Pellin M. J., Lewis R. S., Davis A. M., Amari S. and Clayton R. N. (1998a) Molybdenum isotopic composition of individual presolar silicon carbide grains from the Murchison meteorite. *Geochim. Cosmochim. Acta* **62**, 1093–1104.

Nicolussi G. K., Pellin M. J., Lewis R. S., Davis A. M., Clayton R. N. and Amari S. (1998b) Strontium isotopic composition in individual circumstellar silicon carbide grains: a record of *s*-process nucleosynthesis. *Phys. Rev. Lett.* **81**, 3583–3586.

Nuth J. A., Wilkinson G. M., Johnson N. M. and Dwyer M. (2006) A mechanism for the equilibrium growth of mineral crystals in AGB stars and red giants on 10^5 yr timescales. *Astrophys. J.* **644**, 1164–1170.

Ott U. and Begemann F. (1990) Discovery of *s*-process barium in the Murchison meteorite. *Astrophys. J.* **353**, L57–L60.

Pearce N. J. G., Perkins W. T., Westgate J. A., Gorton M. P., Jackson S. E., Neal C. R. and Chenery S. P. (1997) A compilation of new and published major and trace element data for NIST SRM 610 and NIST SRM 612 glass reference materials. *Geostand. Geoanal. Res.* **21**, 115–144.

Podosek F. A., Prombo C. A., Amari S. and Lewis R. S. (2004) *s*-Process Sr isotopic compositions in presolar SiC from the Murchison meteorite. *Astrophys. J.* **605**, 960–965.

Prombo C. A., Podosek F. A., Amari S. and Lewis R. S. (1993) *s*-Process Ba isotopic compositions in presolar SiC from the Murchison meteorite. *Astrophys. J.* **410**, 393–399.

Rao M. V. (2003) Maturing ion-implantation technology and its device applications in SiC. *Solid State Electron.* **47**, 213–222.

Savina M. R., Davis A. M., Tripa C. E., Pellin M. J., Clayton R. N., Lewis R. S., Amari S., Gallino R. and Lugaro M. (2003) Barium isotopes in individual presolar silicon carbide grains from the Murchison meteorite. *Geochim. Cosmochim. Acta* **67**, 3201–3214.

Savina M. R., Davis A. M., Tripa C. E., Pellin M. J., Gallino R., Lewis R. S. and Amari S. (2004) Extinct technetium in silicon carbide stardust grains: implications for stellar nucleosynthesis. *Science* **303**, 649–652.

Simons D. S., Downing R. G., Lamaze G. P., Lindstrom R. M., Greenberg R. R., Paul R. L., Schiller S. B. and Guthrie W. F. (2007) Development of certified reference materials of ion-implanted dopants in silicon for calibration of secondary ion mass spectrometers. *J. Vac. Sci. Technol. B* **25**, 1365–1375.

Speck A. K., Thompson G. D. and Hofmeister A. M. (2005) The effect of stellar evolution on SiC dust grain sizes. *Astrophys. J.* **634**, 426–435.

Steele I. M., Hutcheon I. D., Solberg T. N., Smith J. V. and Clayton R. N. (1977) Effect of energy selection on quantitative analysis in secondary ion microanalysis. *Int. J. Mass Spectrom. Ion Phys.* **23**, 293–305.

Verchovsky A., Wright I. and Pillinger C. (2004) Astrophysical significance of asymptotic giant branch stellar wind energies recorded in meteoritic SiC grains. *Astrophys. J.* **607**, 611–619.

Virag A., Wopenka B., Amari S., Zinner E., Anders E. and Lewis R. S. (1992) Isotopic, optical, and trace element properties of large single SiC grains from the Murchison meteorite. *Geochim. Cosmochim. Acta* **56**, 1715–1733.

Yin Q., Lee C. and Ott U. (2006) Signatures of the *s*-process in presolar silicon carbide grains: Barium through Hafnium. *Astrophys. J.* **647**, 676–684.

Zinner E. and Crozaz G. (1986) A method for the quantitative measurement of rare earth elements in the ion microprobe. *Int. J. Mass Spectrom. Ion Processes* **69**, 17–38.

Zinner E., Ming T. and Anders E. (1989) Interstellar SiC in the Murchison and Murray meteorites: isotopic composition of Ne, Xe, Si, C, and N. *Geochim. Cosmochim. Acta* **53**, 3273–3290.

Zinner E., Amari S. and Lewis R. S. (1991) *s*-Process Ba, Nd, and Sm in presolar SiC from the Murchison meteorite. *Astrophys. J.* **382**, L47–L50.

Zinner E., Nittler L. R., Gallino R., Karakas A., Lugaro M., Straniero O. and Lattanzio J. (2006) Silicon and carbon isotopic ratios in AGB Stars: SiC grain data, models, and the galactic evolution of the Si isotopes. *Astrophys. J.* **650**, 350–373.

Associate editor: Sara S. Russell